Development and dosimetric verification of 3D customized bolus in radiotherapy

Miss Nichakan Chatchumnan

จุฬาลงกรณ์มหาวิทยาลัย
CHULALONGKORN UNIVERSITY

A Thesis Submitted in Partial Fulfillment of the Requirements

for the Degree of Master of Science in Medical Physics

Department of Radiology

FACULTY OF MEDICINE

Chulalongkorn University

Academic Year 2020

การพัฒนาและตรวจวัดปริมาณรังสีของวัสดุสมมูลเนื้อเยื่อสามมิติในงานรังสีรักษา

น.ส.ณิชกานต์ ชาติชำนาญ

Thesis Title	Development and dosimetric verification of 3D customized bolus in radiotherapy
By	Miss Nichakan Chatchumnan
Field of Study	Medical Physics
Thesis Advisor	Assistant Professor TAWEAP SANGHANGTHUM, Ph.D.
Thesis Co Advisor	Chuanchom Aumnate, Ph.D.

Accepted by the FACULTY OF MEDICINE, Chulalongkorn University in Partial Fulfillment of the Requirement for the Master of Science

.... Dean of the FACULTY OF MEDICINE

(Professor SUTTIPONG WACHARASINDHU, M.D.)

THESIS COMMITTEE

.... Chairman

(Sornjarod Oonsiri, Ph.D.)

.... Thesis Advisor

(Assistant Professor TAWEAP SANGHANGTHUM, Ph.D.)

.... Thesis Co-Advisor

(Chuanchom Aumnate, Ph.D.)

.... External Examiner

(Professor Kosuke Matsubara, Ph.D.)

ณิชกานต์ ชาติชำนาญ : การพัฒนาและตรวจวัดปริมาณรังสีของวัสดุสมมูลเนื้อเยื่อสามมิติในงานรังสีรักษา. (Development and dosimetric verification of 3D customized bolus in radiotherapy) อ.ที่ปรึกษาหลัก : ผศ. ดร.ทวีป แสงแห่งธรรม, อ.ที่ปรึกษาร่วม : ดร.ชวนชม อ่วมเนตร

วัสดุสมมูลเนื้อเยื่อเป็นวัสดุที่เทียบเท่ากับเนื้อเยื่อที่มักใช้เพื่อลดผลกระทบที่ผิวหนังได้รับรังสีในปริมาณน้อยจากการรักษาด้วยรังสีในทางรังสีรักษา วัสดุสมมูลเนื้อเยื่อเชิงพาณิชย์ไม่สามารถวางแนบชิดไปกับพื้นผิวที่มีความโค้งเว้าของผิวหนังของผู้ป่วยได้อย่างสมบูรณ์ส่งผลให้เกิดช่องว่างของอากาศโดยเฉพาะอย่างยิ่งในรูปทรงพื้นผิวที่มีความโค้ง การศึกษาครั้งนี้มีวัตถุประสงค์เพื่อประเมินความเป็นไปได้ของวัสดุสมมูลเนื้อเยื่อที่สร้างขึ้นจากยางซิลิโคนสองชนิดคือ RA-00AB และ RA-05AB ซึ่งทำขึ้นเป็นวัสดุสมมูลเนื้อเยื่อแบบแผ่นเรียบและแบบปรับแต่ง 3 มิติโดยใช้เทคโนโลยีการพิมพ์ 3 มิติ วัสดุสมมูลเนื้อเยื่อความหนา 1 เซนติเมตรถูกสร้างขึ้นจากสารละลายยางซิลิโคนสองชนิด ความแตกต่างของปริมาณรังสีแบบจุดและความแตกต่างของปริมาณรังสีแบบระนาบได้รับการประเมินโดยเปรียบเทียบกับวัสดุสมมูลเนื้อเยื่อเสมือนโดยใช้ดัชนีแกมมาจากซอฟต์แวร์ นอกจากนั้น ประเมินคุณสมบัติทางกายภาพโดยเปรียบเทียบกับวัสดุสมมูลเนื้อเยื่อเชิงพาณิชย์ สำหรับวัสดุสมมูลเนื้อเยื่อแบบ 3 มิติ ทำการออกแบบแม่พิมพ์เพื่อใช้สร้างวัสดุสมมูลเนื้อเยื่อสามมิติ โดยออกแบบที่บริเวณจมูกแก้มและลำคอจากโปรแกรม Fusion 360 จากนั้นพิมพ์แม่พิมพ์ด้วยเครื่องพิมพ์ 3 มิติ และเติมแม่พิมพ์ด้วยสารละลายยางซิลิโคน ผลการวัดปริมาณรังสีของวัสดุสมมูลเนื้อเยื่อแบบสามมิติถูกเปรียบเทียบกับวัสดุสมมูลเนื้อเยื่อในเชิงพาณิชย์โดยใช้วัสดุสมมูลเนื้อเยื่อเสมือนเป็นข้อมูลอ้างอิง ซึ่งความแตกต่างของปริมาณรังสีแบบจุดระหว่างยางซิลิโคนชนิด RA-00AB, ชนิด RA-05AB และ วัสดุสมมูลเนื้อเยื่อเชิงพาณิชย์พบว่าความแตกต่างของปริมาณรังสีแบบจุดมีค่าน้อยกว่า 0.4% ในขณะที่ความแตกต่างของปริมาณรังสีแบบระนาบของยางซิลิโคนทั้งสองชนิด ที่เกณฑ์แกมมา 2% / 2 มิลลิเมตรพบว่ายางซิลิโคนทั้งสองชนิดมีเปอร์เซ็นต์แกมมามากกว่า 99% โดยความหนา, ความหนาแน่น, หน่วย Hounsfield (HU) และการลดทอนปริมาณรังสี ของวัสดุสมมูลเนื้อเยื่อแบบที่สร้างขึ้นเองนั้นค่อนข้างเหมือนกับวัสดุสมมูลเนื้อเยื่อเชิงพาณิชย์ เมื่อวางวัสดุสมมูลเนื้อเยื่อแบบปรับแต่ง 3 มิติลงบนหุ่นจำลองชนิด rando พบว่ามีความแนบชิดพอดีกับรูปทรงพื้นผิวที่มีความโค้งเมื่อเทียบกับวัสดุสมมูลเนื้อเยื่อในเชิงพาณิชย์ อัตราการส่งผ่านแกมมาของวัสดุสมมูลเนื้อเยื่อสามมิติที่สร้างขึ้นเองนั้นสูงกว่าวัสดุสมมูลเนื้อเยื่อเชิงพาณิชย์ สำหรับทุกบริเวณที่ทำการศึกษา แสดงให้เห็นถึงการเพิ่มขึ้นของปริมาณรังสีและความสม่ำเสมอของปริมาณรังสีในอวัยวะเป้าหมายที่มากกว่าเมื่อเปรียบเทียบกับการที่ไม่มีวัสดุสมมูลเนื้อเยื่อ ดังนั้น วัสดุสมมูลเนื้อเยื่อยางซิลิโคนสร้างคุณสมบัติในการวัดปริมาณที่เป็นไปได้เช่นเดียวกับวัสดุสมมูลเนื้อเยื่อเชิงพาณิชย์และสามารถประหยัดต้นทุนได้มากกว่าเมื่อเทียบกับวัสดุสมมูลเนื้อเยื่อในเชิงพาณิชย์ วัสดุสมมูลเนื้อเยื่อแบบสามมิติที่สร้างขึ้นเป็นวัสดุที่ดีในการใช้เพิ่มปริมาณรังสีและสามารถทดแทนและปรับปรุงประสิทธิภาพการรักษาในงานรังสีรักษาได้

สาขาวิชา ฟิสิกส์การแพทย์	ลายมือชื่อนิสิต ....
ปีการศึกษา 2563	ลายมือชื่อ อ.ที่ปรึกษาหลัก ....
	ลายมือชื่อ อ.ที่ปรึกษาร่วม ....

6270007730 : MAJOR MEDICAL PHYSICS
KEYWORD:

Nichakan Chatchumnan : Development and dosimetric verification of 3D customized bolus in radiotherapy . Advisor: Asst. Prof. TAWEAP SANGHANGTHUM, Ph.D. Co-advisor: Chuanchom Aumnate, Ph.D.

Bolus is a tissue equivalent material that is commonly used to reduce the skin-sparing effect in radiotherapy. The commercial flat bolus cannot form perfect contact with the irregular surface of the patient's skin, resulting in an air gap, especially in irregular surface shape. The purpose of this study was to evaluate the feasibility of two types of silicone rubber bolus, RA-00AB, and RA-05AB that were made as to the fabricated flat and 3D customized bolus using 3D printing technology. The 1 cm thick boluses were made from two types of silicone rubber solutions. The point dose and planar dose differences were evaluated by comparing with virtual bolus using gamma index from SNC-patient software. The physical properties were also evaluated by comparing with a commercial one. For the 3D customized bolus, the bolus shell was designed at the nose, cheek, and neck region from the Fusion 360 program. Then print out the shell with the 3D printer and filled the shell with silicone rubber solution. The dosimetric effect of 3D customized bolus was compared to commercial bolus situation by virtual bolus as a reference. The point dose differences between RA-00AB and RA-05AB silicone rubber model compared with commercial bolus were lesser than 0.4%, while the planar dose differences of both models at 2%/2mmm gamma criteria were the same result more than 99% pass. The thickness, density, Hounsfield unit (HU), and dose attenuation of customized bolus were quite the same as a commercial bolus. When a 3D customized bolus was placed on the RANDO phantom, it showed a very good fit against the irregular surface shape compared with the commercial bolus. Gamma passing rate of 3D customized was higher than commercial bolus for all regions, build-up doses increased and the target volume obviously presented more uniform doses compared to the without bolus situation. A silicone rubber bolus produced the feasible dosimetric properties of a commercial bolus and could save cost when compared to a commercial bolus. The 3D printed customized bolus is a good buildup material and could potentially replace and improve treatment efficiency.

Field of Study:	Medical Physics	Student's Signature ....
Academic Year:	2020	Advisor's Signature ....
		Co-advisor's Signature ....

ACKNOWLEDGEMENTS

TABLE OF CONTENTS

LIST OF FIGURES

LIST OF TABLES

LIST OF ABBREVIATIONS

Abbreviations	Terms
3D	Three Dimentional
cGy	Centi-Gray
cm	Centimeter
CTV	Clinical target volume
CT	Computed tomography
cm^3	Cubic centimeter
DTA	Distance to agreement
DTG	Derivative Thermo gravimetry
et al	Et alibi, and others
FTIR	Fourier Transform Infrared Spectroscopy
Gy	Gray
HU	Hounsfield units
Γ	Gamma index
Linac	Linear accelerator
MV	Megavoltage
mm	Millimeter
MU	Monitor unit
PTV	Planning target volume

QA   Quality assurance

SNC   Sun Nuclear Corporation

TPS   Treatment planning system

TGA   Thermogravimetric analysis

TRS   Technical reports series

จุฬาลงกรณ์มหาวิทยาลัย
CHULALONGKORN UNIVERSITY

CHAPTER I

INTRODUCTION

1.1 Background and rationale

Radiotherapy is one of the most common methods used for the treatment of cancer patients. In order to deliver a sufficient radiation dose to the tumor, adequate types and amount of radiation are selected depending on the tumor location. Conventionally, the electron is applied for the treatment of superficial lesions such as skin cancer, while the high-energy photon is used to treat deeply located lesions. With high-energy photon treatment, a sufficient dose cannot be delivered to the surface due to the skin-sparing effect. To avoid this limitation, one occasionally needs to enhance the dose near the surface. Such is a bolus function, a natural or synthetically developed material that acts as a layer of tissue to provide a more effective treatment to the superficial lesions. Materials used as bolus vary from simple water to metal and include various mixtures and compounds. Even with the modernization of the technology for external-beam therapy and the emergence of different commercial boluses,[1] these bolus materials should be nearly tissue equivalent and allow a sufficient surface dose enhancement. [2]

In practice, most commonly used commercial flat boluses cannot form perfect contact with the irregular surface of the patient's skin, particularly the nose, ear, and scalp, and the resulting air gap effects of second skin-sparing effect and reduces both the maximum and surface dose. [3-7]

Thus, commercial flat boluses need to be used with great care, especially when the skin has a particularly irregular shape. Recently, there have been significant advances in 3-dimensional (3D) printing technology. [8, 9] In this study, we fabricated a customized bolus using a 3D printer and assessed whether it could overcome the disadvantages of currently used commercial flat boluses.

1.2 Objectives

1.2.1 To study the bolus characteristics of customized bolus

1.2.2 To compare the dosimetric effects between 3D customized bolus and

commercial bolus

CHAPTER II

REVIEW OF RELATED LITERATURES

2.1 Theory

2.1.1 Bolus

Bolus is a material that has properties equivalent to tissue. It is widely used in practice to make up for missing tissue or to provide a buildup of dose to the skin surface and buildup region. The bolus should be sufficiently flexible to conform to the patient's surface, durable, and cost-effective. [10]

2.1.1.1 Optimal Dose Buildup for Radiation Therapy

Superflab bolus increases the targeted radiation dose during photon and electron treatment by providing scattering of the beam and buildup of the radiation dose at the skin surface. The material was designed to conform completely to a variety of variable surface geometries, eliminating air gaps and further dose absorption.[10]

2.1.1.2 Proven Clinical Usage

The Superflab bolus material as presented in Figure 2.1 has been tested the dosimetric properties that is superior to polystyrene, the previous gold standard in bolus material, when using both photon and electron beams energies. The specific gravity of superflab; being a ratio between density of any matter and density of water, is very similar to that of water at 1.02, approximating tissue-equivalence closer than polystyrene, resulting in broad clinical acceptance.

Figure 2.1: Commercial superflab bolus

2.1.2 Bolus fabrication

In general, two ways have been reported of making a bolus in past studies. One method was to print a bolus directly with 3D printing materials after the design stage. Polylactic acid (PLA), whose physical density was 1.19 g/cm^3, was a commonly used printing material, which had been demonstrated to be a bolus material in a previous study.[11] Studies reported that the doses of 3D printed PLA bolus in phantom simulating breast cancer radiotherapy after radical resection were more uniform than with the commercial bolus.[12, 13] Acrylonitrile butadiene styrene (ABS) copolymer is another printing material commonly used except PLA, but both materials are too hard and have poor comfort. More importantly, the different infill percentages of these two materials correspond to different densities, leading to discrepancies between the calculated and measured dose distribution. Another method is to print the shell of the bolus and then fill it with other soft materials. Richard et al.[14] printed the shell in PLA using the 3D printer and filled it with silicone rubber for non‑melanoma skin cancer electron beam radiotherapy. Silicone rubber has advantages when making a bolus due to its excellent biocompatibility, chemical stability, and good mechanical properties.

2.1.3 Three-dimensional printing technology

2.1.3.1 Basic definition [15]

3D printing is a manufacturing process that creates a three-dimensional object by incrementally adding material until the object is complete (this contrasts with subtractive manufacturing techniques such as carving or milling, in which an object is created by selectively removing parts from a piece of raw material). A 3D printer is simply a machine that can take a digital 3D model and turn it into a tangible 3D object via additive manufacturing. The example of a 3D printer machine is shown in Figure 2.2.

Figure 2.2: 3D Printer machine

2.1.3.2 Types of 3D printing

There are many types of 3D printing techniques used in various industries, such as

1. Fused Deposition Modeling (FDM): FDM uses a simple nozzle to extrude plastic filaments, which cool down into the 3D printed shape, as shown in Figure 2.3. This is the cheapest version of 3D printing technology and the kind available to consumers. Since it only needs a box, a nozzle, and a system to turn the digital data into movement, this type of printer can come in many different sizes.

2. Stereolithography (SLA): Technically the first type of 3D printing to be invented back in the 1980s, SLA beams a laser at a reactive liquid resin, so it instantly hardens. The object is then pulled out of a vat of this liquid, layer by layer. As a result, SLA is capable of much greater details than FDM, but the printing process is also more complex.

3. Selective Laser Sintering (SLS): This type of 3D printing technique starts with powdered materials with very specific properties, such as polyamides and thermoplastic elastomers. It uses a powerful laser to rapidly fuse (not melt) these powders into the correct layers, forming a very durable object. This industrial version of 3D printing is very useful for mass-producing functional parts or prototypes.

4. Metal printing: Printing types like selective laser melting (SLM) and electron beam melting (EBM) use welding-like techniques to create objects. This printer moves a platform down slowly as layers of powdered metal are added and dissolved with incredible precision. This type of printing takes very powerful lasers and a controlled environment, so it is not usually seen outside of situational industrial manufacturing.
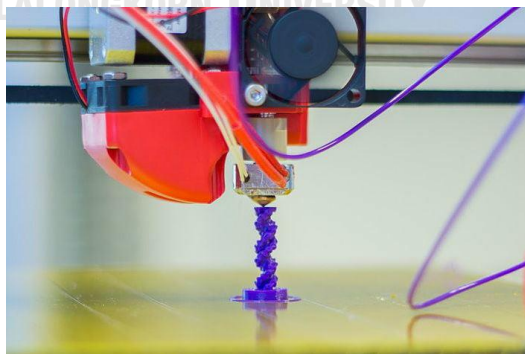
Figure 2.3: Fusion Deposition Modeling (FDM) printing

2.1.4 Gamma Evaluation

The Gamma Index is essential to estimate the point-by-point difference between measured and calculated dose distribution in terms of both Distance to Agreement (DTA) and Dose Difference (DD). The distance between reference point and the closest data point in the compared dose distribution that manifests the same dose is defined as DTA[16]. The composite analysis of DTA and DD is needed to work in both high and low dose gradient regions because DTA measure performs well only in high dose gradient regions. When passing both DD and DTA criteria, the test is passed. Moreover, the patient plan is accepted when the index value is ≤ 1 by its formula and when γ value is greater than one, plan is rejected [17]. Measured dose distributions were compared with the calculated ones using the gamma index method by applying the global normalization at 3%/2mm according to AAPM TG-218 and acceptance criteria in this study was set at 90% pass. Thus, the percentage of dose points was measured that satisfy acceptance criteria can determine the goodness of treatment plan. The gamma method, as prepared by Low et al.[18], was designed for the two-dose distribution comparison: one is defined to be the reference information ($D_r(r)$) and the other is queried for evaluation ($D_c(r)$).

Figure 2.4 represents a schematic of the gamma analysis tool for two-dimensional dose distribution evaluations. The acceptance criteria are denoted by ΔD_M for the dose difference and Δd_M for the distance to agreement (DTA). For a reference point at position r_r, receiving dose D_r, the surface representing these acceptance criteria is an ellipsoid defined by equation 2.1.

$$\Gamma = \sqrt{\frac{\Delta d^2}{\Delta d_M^2}} + \sqrt{\frac{\Delta D^2}{\Delta D_M^2}}$$

(2.1)

Where $\Delta r = | r_r - r_c |$ is the distance difference between the reference and compared point and $\Delta D = D_c(r_c) - D_r(r_r)$ is the dose difference at the position r_c relative to the reference dose D_r in r_r. For the compared distribution to match the reference dose in

r_r, it needs to contain at least one point (r_c, D_c) lying within the ellipsoid of acceptance, i.e., one point for which:

$$\Gamma_r(r_c, D_c) = \sqrt{\frac{\Delta d^2}{\Delta d_M^2}} + \sqrt{\frac{\Delta D^2}{\Delta D_M^2}}$$

A quantitative measure of the accuracy of the correspondence is determined by the point with the smallest deviation from the reference point, i.e., the point for which $\Gamma_r(r_c, D_c)$ is minimal. This minimal value is referred to as the quality index $\gamma_{(r_r)}$ of the reference point.

The pass-fail criterion therefore becomes:

$\gamma_{(r_r)} \leq 1$, correspondence is within the specified acceptance criteria,

$\gamma_{(r_r)} > 1$, correspondence is not within specified acceptance criteria.

An implicit assumption is performed that once the passing criteria are selected, DD and DTA analyses have equivalent significance when determining calculation quality.
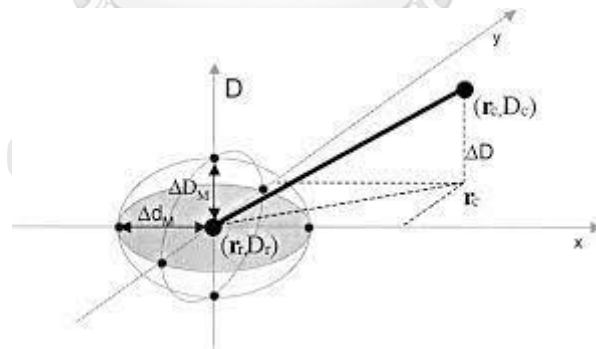
Figure 2.4 Schematic representation of the theoretical concept of

the gamma evaluation method

2.2 Review of related literature

Shin wook kim et al, [19] fabricated a customized 3D bolus using a 3D printer, as displayed in Figure 2.7. They evaluated its feasibility in clinical practice by comparing its performance without a bolus in the treatment planning system. The 3D printed bolus is a good fit against the irregular surface of the RANDO phantom and the resulting dosimetric parameters of the plan without a bolus and with the 3D printed customized bolus on the surface of the RANDO phantom.

The result showed that the 3D printed flat bolus could provide effective dose coverage in the buildup region. The d_{max} of the plan with the superflab and 3D printed flat bolus were shifted toward the surface of the Blue water phantom by as much as 0.91 cm and 0.85 cm, respectively. There were slight differences between the dosimetric results obtained using these boluses because the 3D printed flat bolus is not identical to the superflab bolus with respect to its HU value and density. At 120 kVp, the HU of the 3D printer bolus was -123.6±18.2 HU compared to -33.04±7.6 HU for the superflab bolus. In addition, the commercially available flat boluses and the 3D printed flat bolus also do not have completely homogeneous HU values, potentially giving rise to variation in the measured doses at the central axis.

Furthermore, the treatment plan with the 3D printed customized bolus could be clinically effective, help overcome the problem of variable air gaps, and improve the reproducibility of daily setup conditions on irregular surfaces compared to commercial flat boluses.

Figure 2.5: The 3D printed customized bolus on the surface of the RANDO phantom

Yuehong Kong et al. [20] used 3D printing skills to create individually customized boluses designed to compensate for the irregular surface in photon IMRT radiotherapy. The dosimetric differences of hydrogel, silica gel, and commercial boluses were compared in head phantoms simulating nose, ear, and parotid gland radiotherapy. Hydrogel is flexible, odorless, biologically nontoxic, and highly transparent, but it has not been used as a bolus in radiotherapy because of its physical characteristics. Hydrogels tend to lose water and undergo deformation, which is not suitable for long-time use. The traditional polymer hydrogel is usually formed by chemical cross-linking. The uneven dispersion of the chemical cross-linking agent leads to an irregular gel network, and the gel is very fragile, which dramatically limits its application[21, 22].

The polyol polyurethane membrane was used to cover the hydrogel surface to prevent contact with air, thereby preventing dehydration. Because of its poor strength, many studies reported the methods to increase its strength, such as nanocomposite hydrogel [23, 24] and double-network hydrogel [25-27] Clinical application of strong, tough, and responsive hydrogels is the future development direction, but more improvement is needed in biosafety and biocompatibility. Most of the novel hydrogels have strong hydrophilicity, which is not conducive to affinity with cells or biological tissues. Therefore, how to improve the biological function of hydrogel is also a problem to be overcome, or polymeric gel could be used, which has been reported to have been used for bolus [28].

However, the results found that Silica gel and hydrogel boluses were suitable for fit and a high level of comfort and repeatability and had better dose parameters in IMRT plans. Therefore, they may replace the commercial bolus for clinical use.
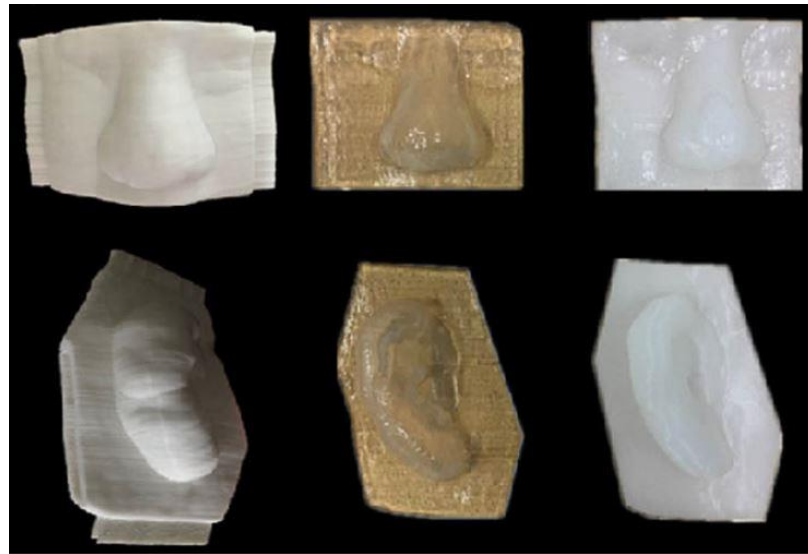
Figure 2.6: The procedure of making hydrogel and silica gel boluses based on 3D
printing technology. (a) The bolus shell fabricated by

3D printing, (b) hydrogel bolus, (c) silica gel bolus.

Jae Won Park et al. [29] used a three-dimensional (3D)-printed customized bolus
(3D bolus) for radiotherapy application to irregular surfaces. They said that the bolus
fabrication based on computed tomography (CT) scans complicated and also delivers
unwanted irradiation. Consequently, they fabricated a bolus using a 3D scanner and
evaluated its efficacy. The head of an Alderson Rando phantom was scanned with a
3D scanner. The 3D surface data were exported and reconstructed with Geomatic
Design X software. A 3D bolus of 5-mm thickness designed to fit onto the nose was
printed with rubber-like printing material, and a radiotherapy plan was developed.
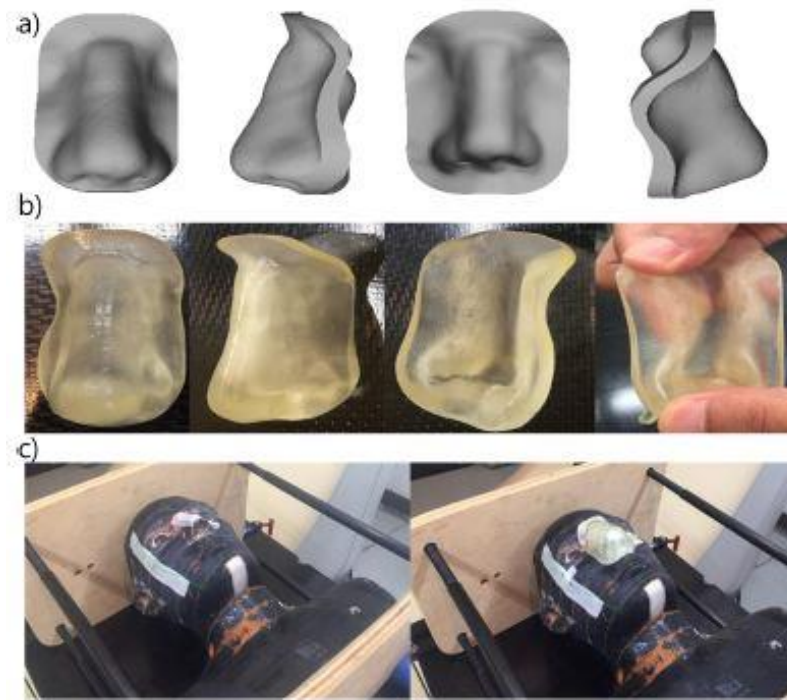
Figure 2.7: 3D bolus fabricated with 3D scanner

(a) STL file view of the designed 3D bolus

(b) 3D printed obtained with malleable material, Tango Plus

(c) CT simulation scan setup of the bolus on the Rando phantom.

They successfully fabricated the customized 3D bolus, and further, a CT simulation indicated an acceptable fit of the 3D bolus to the nose. There was no air gap between the bolus and the phantom surface. The percent depth dose (PDD) curve of the phantom with the 3D bolus showed an enhanced surface dose compared with that of the phantom without the bolus. The PDD of the 3D bolus was comparable with that of a commercial superflab bolus.
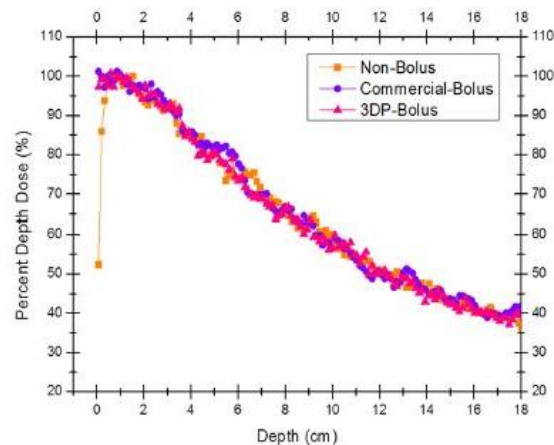
Figure 2.8: Percent depth dose (PDD) analysis with the use of Gafchromic EBT film.

The 3D-printed bolus sufficiently enhanced the surface dose, and its PDD was comparable with that of a commercial flat bolus. The PDD without a bolus shows significant under-dosing to the surface area. The build-up effect is considered a significant benefit of megavolt photon beams because of a reduction in the skin dose, resulting in reduced skin toxicity. However, this effect can jeopardize target coverage of superficial tumors, and therefore, a commercial bolus is commonly used in such situations to increase the surface dose in radiation oncology clinics[1]. However, difficulties in fitting a commercial bolus can result in unwanted air gap formation over irregular surfaces, which can be detrimental to radiotherapy planning; a previous study reported that a 10-mm air gap has resulted in a 10% reduction in the surface dose[4].

The radiotherapy plan considering the 3D bolus showed improved target coverage when compared with that without the bolus. Thus, they successfully fabricated a customized 3D bolus for an irregular surface using a 3D scanner instead of a CT scanner.

CHAPTER III

RESEARCH METHODOLOGY

3.1 Research design

This research was observational design in the type of analytical study.

3.2 Research design model

This research was divided into two major steps. The first step was bolus characteristics. The second was a clinical application diagram to compare the dosimetric effect between various types of the bolus—figures 3.1 and 3.2 display the diagram of each step in this research according to the above explanation.

3.2.1 Bolus characteristics
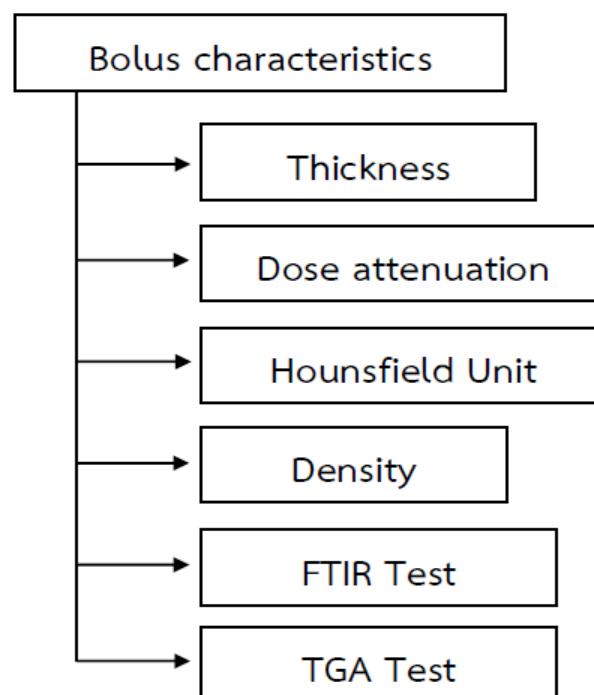
Figure 3.1 Research design model of bolus characteristics

3.2.2 Clinical application
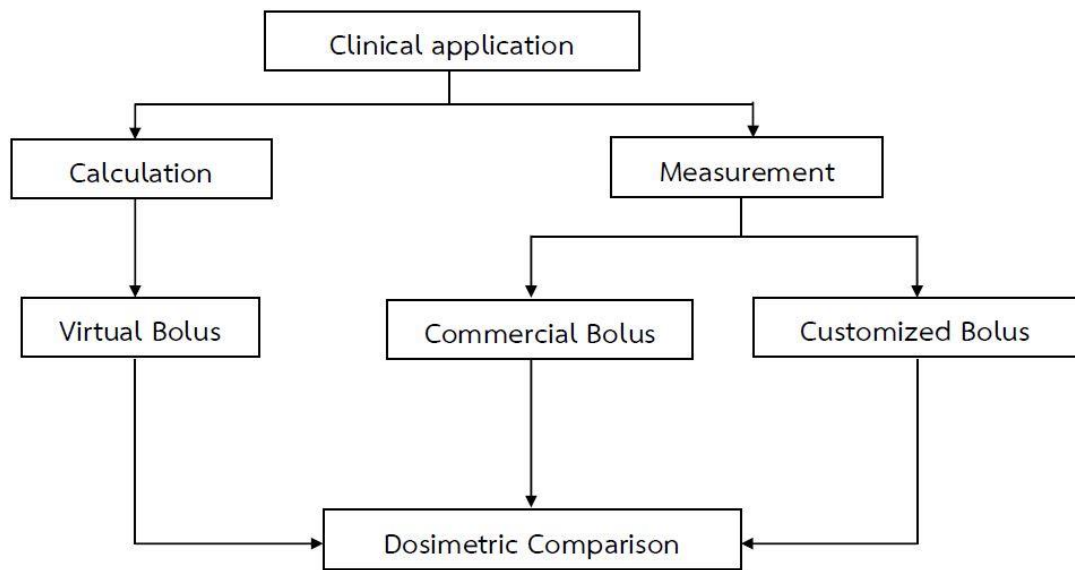
Figure 3.2 Research design model of clinical application

3.3 Conceptual framework

Dosimetric effect was affected by several factors as shown in figure 3.3.
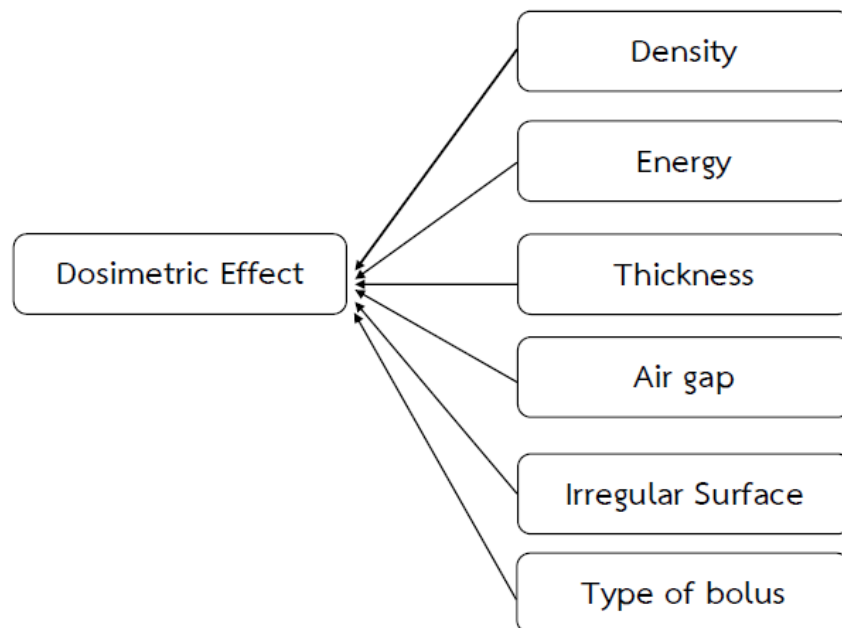
Figure 3.3 Conceptual framework

3.4 Research questions

3.4.1   What are the bolus characteristics of customized bolus?

3.4.2   What are the dosimetric effects between 3D customized bolus and commercial bolus?

3.5 Materials

The materials used in this study were supplied from the Division of Radiation Oncology, King Chulalongkorn Memorial Hospital.

3.5.1 Silicone rubber solution, model RA-00AB and RA-05AB

Silicone rubber solution, model RA-00AB (Rungart, company, Bangkoknoi, Bangkok) is a composition of Vinyl silicone oil and white carbon black, while model RA-05AB is based on Hydroxy-terminated Polydimenthylailoxane, Aqua and Titanium Dioxide. One set of silicone rubber solution consists of component A and B as shown in figure 3.4.

(a)   (b)

Figure 3.4: Silicone rubber solution of (a) RA-00AB, (b) RA-05AB.

3.5.2 Digital weighting machine

The digital weighting machine in figure 3.5 is used to weight the silicone rubber solution in a ratio of 1:1 for mixing the solution.

Figure 3.5: Digital weighting machine

3.5.3 Solid water phantoms

The solid water phantoms (Gammex, Middleton, WI) with 30x30 cm^2 in sizes and various thicknesses from 2 mm to 5 cm as displays in figure 3.6 are used to measure the dosimetric effect by FC65-P detector.

Figure 3.6: Solid water phantom

3.5.4 Anthropomorphic RANDO® phantom

Anthropomorphic RANDO® phantom (The Phantom Laboratory, Salem, NY, USA), as exhibited in figure 3.7, is molded of tissue-equivalent material. RANDO® phantom incorporates the materials to simulate various tissues such as muscle, bone, lung, and air cavity. RANDO® phantom provides the detailed mapping of dose distribution that is essential for evaluating radiotherapy treatment plans. There are two RANDO® models: RANDO® Man and RANDO® Woman. RANDO® phantoms are

constructed with a natural human skeleton cast inside the radiologically equivalent material to soft tissue. RANDO® phantom is transected-horizontally into 2.5 cm thick slices. Each slice has holes that are plugged with bone equivalent, soft tissue equivalent, or lung tissue equivalent pins and can be replaced by TLD holder pins for in vivo dosimetry. [28, 29]

Figure 3.7: Anthropomorphic RANDO® phantom

3.5.5 The create bot D600 3D printer

The create bot D600 3D printer (Suwei Electronic Technology Co., Henan, China) is equipped with the 4th generation 1.75mm dual extruders and hot ends. The left extruder is equipped with 260°C hot end; It can print with PLA, ABS, PC, Nylon, Carbon fiber, Flexible. The right extruder 420°C hot end is made of martensite steel, which can print high-performance materials. Moreover, the extruder feeding system support high-speed printing, and accuracy can reach high to 0.05mm. The 3D printer is used to print out the 3D bolus shell for making a 3D customized bolus, as shown in figure 3.8.

Figure 3.8: The create bot D600 3D printer

3.5.6 The FC65-P detector

The FC65-P (IBA Dosimetry GmbH, Schwarzen-Bruck, Germany) is a farmer-type ionization chamber that is intended for the absolute dosimetry of photon and electron beams at therapy level dose rates. Furthermore, these chambers are suitable for dosimetry in proton fields and for depth dose measurements and field profile analysis. When calibrated accordingly, these chambers can be used for measuring the quantities absorbed dose to water, absorbed dose to air, air kerma, or exposure in air, depending upon the type and quality of radiation and the relevant code of practice.

The watertight chamber consists of a conducting plastic thimble and a pure aluminum inner electrode, supported by a thin aluminum stem. The stem terminates in a robust cable entry where the chamber is fixed on the appropriate chamber holder. The inner diameter of the outer electrode is 6.2 mm, the inner electrode length is 20.5 mm, and the sensitive volume is 0.65 cm3, as shown in figure 3.9.

Figure 3.9: The FC65-P detector [13]

3.5.7 Electrometer

To measure the collection charge during the output measurement, the Dose1 Electrometer (Wellhofer Dosimetry, Schwarzenbruck, Germany), as shown in figure 3.10 was connected to each detector. This electrometer is able to measure the electrical charge in the range from 40 pC to 1.0 C at the resolution of 0.1 pC. The ion collection charge will be visualized clearly in the digital number. This type of electrometer is convenient for the use of ionization chambers, diode detectors, as well as diamond detectors.

Figure 3.10: Electrometer

3.5.8 Gafchromic film

The Gafchromic EBT^3 film (Ashland Inc., Wayne, NJ, USA), which is shown in figure 3.11, is an ideal medium for quantitative dosimetric. The spatial resolution is better than 0.1 mm and the response is energy and fractionation independent. The EBT film is self-developing and can be handled in room light.
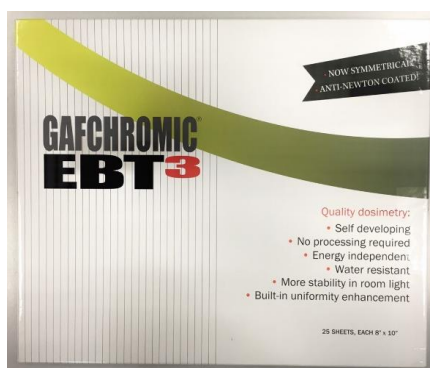
Figure 3.11: Gafchromic EBT^3 film

3.5.9 Film scanner

The Epson Perfection V700 flat-bed color CCD (Epson America, Inc., USA), which is shown in figure 3.12, for EBT film digitization is used as a scanner. The maximum support of media size is 22x30 cm^2. The color depth of scanner is 48-bit color. The optical resolution of scanner is 6,400 dpi x 9, 600 dpi and the maximum resolution is 12,800 dpix12, 800 dpi of interpolated resolution.

Figure 3.12: The film scanner (Epson perfection v700 photo)

3.5.10 Eclipse^{TM} treatment planning system

Eclipse^{TM} treatment planning system software Version 15.6, (Varian Medical System, Inc., Palo Alto, CA, USA) as shown in figure 3.13 is an integrated and comprehensive treatment planning system to support the external beam Radiation therapy such as photon (3D-CRT, IMRT, VMAT technique), electrons, protons, low-dose-rate brachytherapy, and cobalt therapy. There are two photon dose calculation algorithms: Analytical Anisotropic Algorithm (AAA) and Acuros XB algorithm. The AAA algorithm was used to calculate the head and neck dose distribution in this study, Eclipse^{TM} TPS allows clinicians to efficiently create the organs and calculate the best treatment plans for their patients[30].
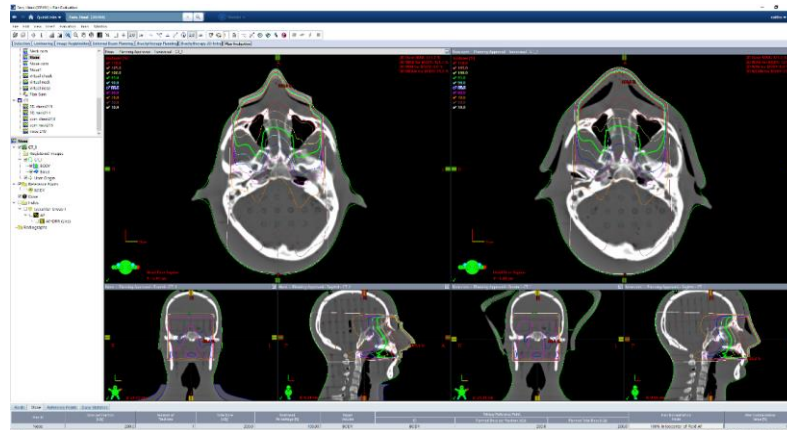
Figure 3.13: Eclipse[TM] treatment planning system software

3.5.11 Sun Nuclear Patient software

The advanced treatment technique such as IMRT and VMAT requires the patient-specific QA to verify the accuracy of MLC movement in each patient. Modern patient plans are often collections of small beamlets with very steep dose gradients. Since these dose gradients are tightly conformed to patient anatomy and PTV, accurate verification of the dose gradient is critical. SNC patient software (Sun Nuclear Corporation, Melbourne, FL, USA) can compare the plane or volume dose difference and presents in terms of gamma passing rate as shown in figure 3.14. This research employed SNC software to evaluate 2D planar dose difference at the central axis[31].
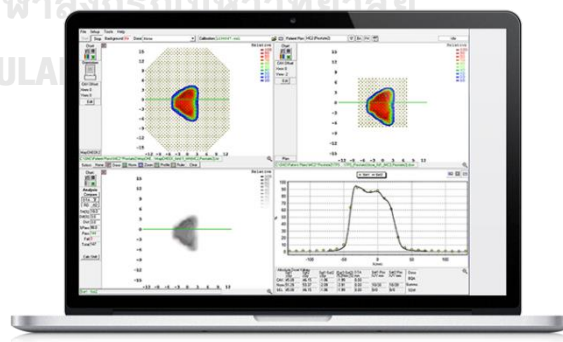
Figure 3.14: SNC patient software

3.5.12 CT simulator

The DECT simulator (SOMATOM Definition AS 64-slice configuration, Siemens Healthcare GmbH, Erlangen, Germany) as shown in figure.3.15, was used in this study. Aperture bore diameter size of 800 mm is designed for immobilization insertion. The

distance from tube to isocenter is 595 mm. The distance from tube to detector is 1085 mm. Tube voltage setting is 80, 120, 140 kVp and 80/140 kVp combination for DECT option. The range of mA setting is 20-666 mA. The reconstruction matrix size is 512x512.
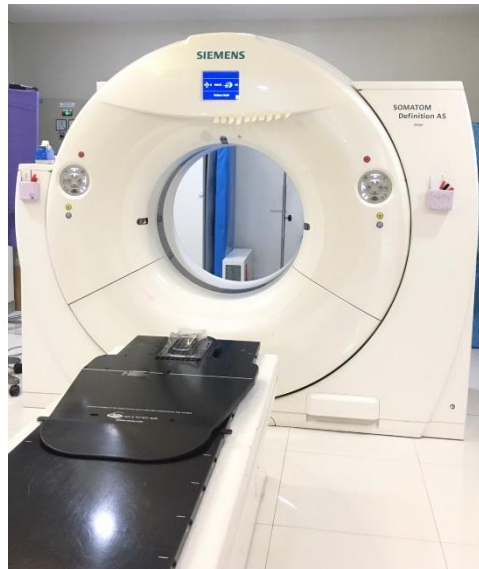
Figure 3.15: Dual-energy CT
(Siemens-SOMATOM Definition AS (64-slice configuration))

3.5.13 Linear accelerator

Linear accelerator or Linac is the external beam radiation treatments machine. A linear accelerator is used to treat cancer patients. It can deliver high-energy electrons to the region of the patient's tumor. This research employed Varian TrueBeamTM linear accelerator (Varian Medical System, Palo Alto, CA, USA), as shown in figure 3.16. The linear accelerator provides all forms of advanced external beam radiotherapy, including 3D-CRT, IMRT, and VMAT techniques. This Varian TrueBeamTM linear accelerator provides two photon energies: 6 MV and 10 MV in both flattened and unflattened photon beams. The electron beams are also provided in various energies: 6, 9, 12, 15, 18, and 22 MeV with 120-leaf multileaf collimators (MLCS).

The on-board imaging (OBI', Varian Medical System, Palo Alto, CA, USA) is mounted on a gantry as the robotic arm on the Varian TrueBeamTM Linear accelerator system. It consists of a kV X-ray source (KVS) and a kV amorphous-silicon digital imaging

detector (KVD). The CBCT images were reconstructed using about 700 kV-projection images acquired over 360°rotation and reconstructed post-processing image by filter back projection. When the center of the KVD is positioned at the isocenter in the longitudinal-lateral plan and 50 cm away from the isocenter in the vertical direction, the reconstructed field-of-view (FOV) is a circle of 24 cm diameter with a 15 cm length. This acquisition mode is called "full - fan" and is used for small anatomic sites such as the brain, head-and-neck, and a truncated part of more significant sites.

For larger sites, such as the pelvis, chest, and abdomen only part of the object is viewed in a half-fan projection and the other part of the object is viewed in the half-fan projection from the opposite direction. This acquisition mode is called 'half-fan'. The FOV for the half-fan method is a circle of 45 cm diameter with a 14 cm length. The effects of X-ray scatter and artifacts are larger in CBCT images than in CT images. A bowtie filter is mounted to the X-ray tube to improve image quality by reducing intensity variations across the detector.

Figure 3.16: Varian TrueBeam^{TM} linear accelerator
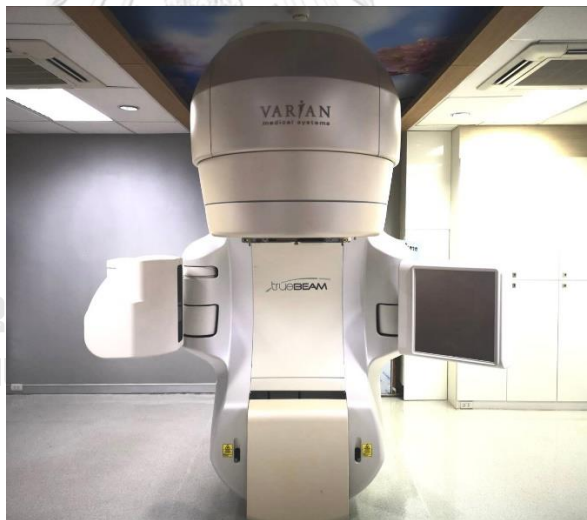
3.5.14 Fourier Transform Infrared Spectrometer

Fourier Transform Infrared Spectrometer as shown in Figure 3.17, also known as FTIR Analysis or FTIR Spectroscopy, is an analytical technique used to identify organic, polymeric, and, in some cases, inorganic materials. The FTIR analysis method uses infrared light to scan test samples and observe chemical properties[32].

Figure 3.17: FTIR Scanning Microscope

The FTIR instrument sends infrared radiation of about 10,000 to 100 cm^{-1} through a sample, with some radiation absorbed and some passed through. The absorbed radiation is converted into rotational and vibrational energy by the sample molecules. The resulting signal at the detector presents as a spectrum, typically from 4000 cm^{-1} to 400 cm^{-1}, representing a molecular fingerprint of the sample, as shown in Figure 3.18. Thus, each molecule or chemical structure will produce a unique spectral fingerprint, making FTIR analysis an excellent tool for chemical identification.

FTIR spectroscopy is an established technique for quality control when evaluating industrially manufactured material and can often serve as the first step in the material analysis process. A change in the characteristic pattern of absorption bands clearly indicates a change in the composition of the material or the presence of contamination. This technique is helpful for analyzing the chemical composition of smaller particles, typically 10 to 50 microns, as well as larger areas on the surface.
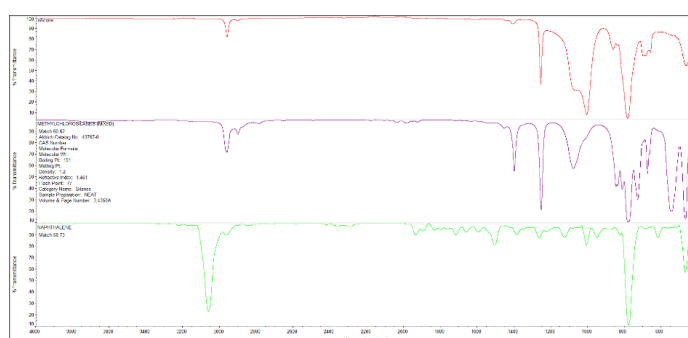

Figure 3.18: FTIR Spectrograph

3.5.15 Thermogravimetric analyzer

Thermogravimetric analysis (TGA) is conducted on an instrument referred to as a thermogravimetric analyzer. A thermogravimetric analyzer continuously measures mass while the temperature of a sample is changed over time. This measurement provides information about physical phenomena, such as phase transition, absorption, and desorption[33]. The example of the TGA machine is shown in Figure 3.19.

TGA can be used to evaluate the thermal stability of a material. If a species is thermally stable in the desired temperature range, there will be no observed mass change. Negligible mass loss corresponds to little or no slope in the TGA trace. TGA also gives the upper use temperature of a material. Beyond this temperature, the material will begin to degrade.

TGA is used in the analysis of polymers. Polymers usually melt before they decompose; thus, TGA is mainly used to investigate the thermal stability of polymers. Most polymers melt or degrade before 200 °C. However, a class of thermally stable polymers can withstand temperatures of at least 300 °C in air and 500 °C in inert gases without structural changes or strength loss, which TGA can analyze.

Figure 3.19: Thermogravimetric Analyzer

3.6 Methods

The methods were divided into three sections. The first part was to fabricate the customized bolus. The second section was to evaluate the characteristics of the bolus. The last part was the section on comparing dosimetric effect in the clinical part.

3.6.1 Bolus fabrication

The 1 cm boluses produced from two kinds of silicone rubber solutions (RA-00AB and RA-05AB) with the size of 10×10 cm^2 were evaluated in dosimetric from point dose differences at 0.5, 1.0 and 1.5 cm depths and planar dose differences at 1.5 cm depth by comparing with virtual bolus created in Eclipse treatment planning system (TPS) (Varian Medical Systems, Palo Alto, CA) using gamma index from SNC-patient software (Sun Nuclear Corporation, Melbourne, FL).

Fig. 3.20: The silicone rubber solution of (a) RA-05AB, (b) RA-00AB
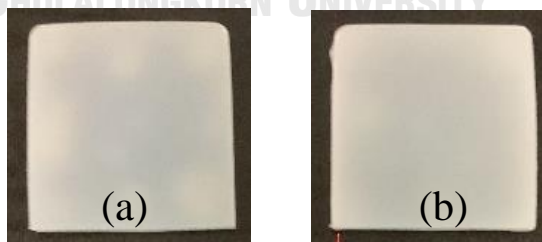
Fig. 3.21. The silicone rubber bolus of (a) RA-05AB size, (b) RA-00AB.

3.6.1.1 Flat customized bolus fabrication

The bolus presented better dosimetric results. The RA-00AB model was selected to fabricate a flat bolus with the size of 30×30 cm^2. The procedures of fabrication flat bolus were to mix the silicone rubber solution (RA-00AB) A and B weight in a ratio of 1:1 by digital weighing machine then pour into the container with size of 30x30x1 cm^3 and keep in the room temperature for 24 hr. Then the flat customized are shown in figure 3.22.

Figure 3.22: Flat customized bolus with size of 30x30x1 cm^3

3.6.1.2 3D customized bolus fabrication

The procedures of fabrication 3D customized bolus were as followings:

1. The three pieces of bolus shells were designed by 3D slicer and Fusion 360 program, as shown in figure 3.23.
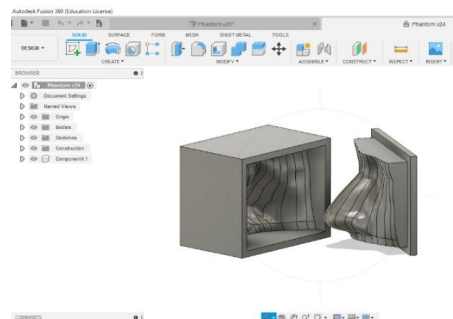
Figure 3.23: The design of 3D bolus shell for nose region

2. The STL file of 3D bolus shells were printed by the 3D printer (Create Bot D600 Printer), as shown in figure 3.24.
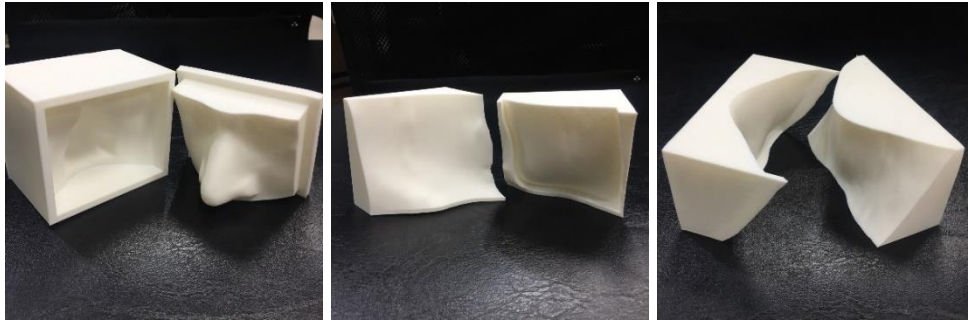
Figure 3.24: 3D bolus shell for difference region
(a) nose region, (b) cheek region and (c) neck region

3. The silicone rubber solution was filled into the shell. The three pieces of 3D customized bolus are shown in figure 3.25.
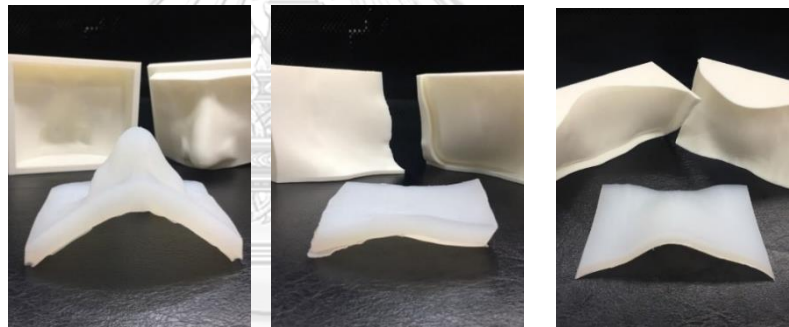
Figure 3.25: 3D customized bolus for difference region
(a) nose region, (b) cheek region and (c) neck region

3.6.2 Bolus characteristics

The bolus characteristics of flat customized bolus with size of 30x30x1 cm^3 such as thickness, density, Hounsfield unit (HU), and dose attenuation, were also confirmed and compared to commercial flat bolus.

3.6.2.1 Thickness

The thickness of customized bolus was measured by vernier caliper for 4 positions of bolus.

3.6.2.2 Dose attenuation

The dose attenuation verification of bolus was measured by FG65-P detector in solid phantom at 5 cm depth, 6MV photon beams, 10×10 cm^2 field and SAD technique as presented in figure 3.26.

Figure 3.26: The dose attenuation measurement setting up for
(a) commercial bolus, (b) customized bolus

3.6.2.3 Hounsfield unit

The HU of the bolus was measured for 9 positions on Eclipse treatment planning system (TPS).

3.6.2.4 Density

The density was calculated using the density formula as shown in equation 2.3

$$\rho = \frac{m}{v} \tag{2.3}$$

Where m is mass, while v is volume

3.6.2.5 ATR - FTIR Test

Attenuated total reflection Fourier transform infrared spectroscopy (ATR-FTIR) was used to compare the composition between irradiation and non-irradiation of the bolus. The equipment: ATR-FTIR (PerkinElmer spectrophotometer100), scanning in the range of 4000-500cm^{-1}, with a resolution of 4 cm^{-1}.

3.6.2.6 TGA Test

The TGA Test was used for evaluating the stability of the bolus after irradiation. The thermal stability data was obtained using NETZSCH TG209 F3 thermogravimetric analyzer under linear temperature range of 35-600 °C at a heating rate of 10 °C/min in a nitrogen atmosphere.

3.6.3 Clinical application

The clinical application consists into two parts, point dose difference and planar dose difference.

3.6.3.1 Point dose difference

The procedures of measurement point dose differences were as followings:

1. The Gafchromic film EBT^3 was cut along the shape of rando phantom in 3 regions: nose, cheek and neck as shown in figure 3.27. The 2 slices of rando phantom were used for each region. Therefore, the 2 sets of films were prepared to use with 2 types of boluses.

(a)   (b)   (c)

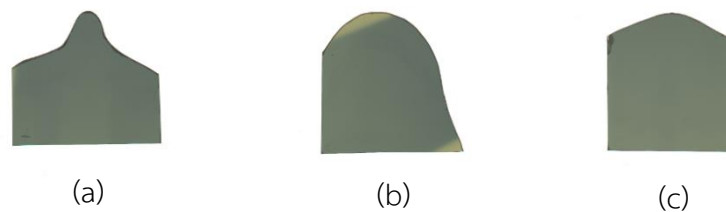**Figure 3.27:** Gafchromic film EBT^3 for use with difference region

(a) nose region, (b) cheek region and (c) neck region

2. The films were arranged at suitably region in rando phantom.

3. The rando phantom with bolus was positioned on the couch of linear accelerator as shown in figure 3.28 using the wall lasers or field light for alignment. The lateral phantom was set by longitudinal laser and vertical lasers.
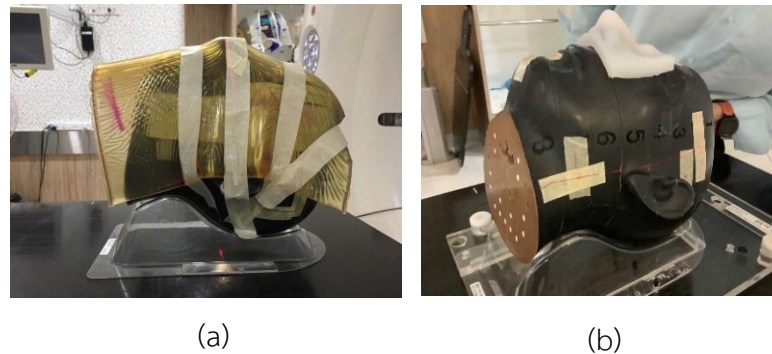
| (a) | (b) |

Figure 3.28: The gafchromic film EBT^3 measurement of boluses for
(a) commercial bolus, (b) 3D customized bolus.

4. The film scanner was used to scan the films and readout the point dose at central axis of commercial bolus and 3D customized bolus by Sun Nuclear Patient software.

5. The central axis dose plane of virtual bolus plan was exported from Eclipse TPS and imported to Sun Nuclear Patient software to readout the point dose at the same point as commercial bolus and 3D customized bolus.

6. Data analysis were performed by the percentage of dose difference for any region of 2 types of boluses and virtual bolus. The percentage of dose difference of 2 types of boluses and virtual bolus were analyzed by equation,

$$\text{Dose difference (\%)} = \frac{Dose\ of\ commercial\ bolus\ or\ Dose\ of\ 3D\ bolus\ -\ Dose\ of\ virtual\ bolus}{Dose\ of\ virtual\ bolus} \times 100$$

3.6.3.2 Planar dose difference

The procedures of measurement planar dose differences were as followings:

1. Anthropomorphic RANDO® phantom with commercial bolus and 3D customized bolus was positioned on the couch of CT simulator using a laser system to set up the phantom at the isocenter position. The lateral phantom was set by longitudinal laser, and vertical lasers set the vertical direction of the phantom with an isocenter at the nose, cheek, and neck region.

2. The phantom was scanned by a CT simulator.

3. The 3D original plans from the patient's treatment plans were transferred and recalculated in the treatment planning system.

4. The dose plane of commercial bolus, 3D customized bolus, and virtual bolus were exported from Eclipse TPS and imported to Sun Nuclear Patient software. The 2D dose plane from the planning of boluses was compared in terms of gamma index (3%/2mm), which virtual bolus was used as a reference as shown in figure 3.29.
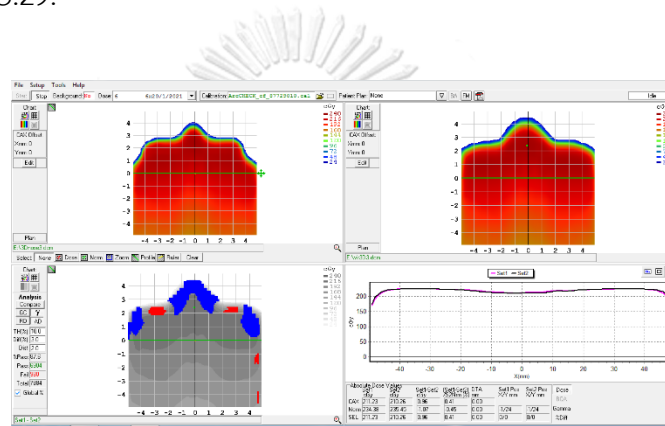
Figure 3.29: The gamma passing rate in Sun Nuclear Patient software

3.7 Statistical analysis

1. Maximum, minimum, mean, and standard deviation were used to present the results.

2. The percent dose difference define as
$$\left(\frac{Dose\ of\ 3D\ bolus\ or\ Dose\ of\ commercial\ bolus\ -Dose\ of\ virtual\ bolus}{Dose\ of\ virtual\ bolus}\right) \times 100 \quad \text{was}$$
applied to compare the dosimetric of various types of boluses

3. The Paired T-test was applied to compare the percentage dose difference between 3D customized bolus and commercial bolus.

3.8 Sample size determination

This research fabricated three pieces of bolus to use with different regions include nose, cheek, and neck regions is an area that is actually clinical use.

3.9 Outcome measurement

This research measured the dosimetric effect of 3D customized bolus.

3.10 Benefits of research

With the same properties of commercial bolus, the 3D customized bolus is expected to improve the efficiency of radiation treatment in cases of superficial tumor in irregular shape surface with the better contact of bolus to patient's skin compared with commercial bolus.

3.11 Ethical consideration

This research involves the dosimetric effects between various types of bolus. The patient plan data were collected and recalculated in phantom on treatment planning system. The research proposal was submitted and approved by Ethic Committee of Faculty of Medicine, Chulalongkorn University, and Bangkok, Thailand (IRB NO.416/63). The certificate is shown in APPENDIX.

CHAPTER IV

RESULTS

The results were separated into three parts: the bolus fabrication, the bolus characteristics, and clinical application for dosimetric comparison between various types of the bolus.

4.1 Bolus fabrication

For the point dose differences, both RA-05AB and RA-00AB bolus showed less than 0.4% dose deviation from commercial bolus for all depths, as presented in Table 4.1. The dose attenuation of both types of bolus were quite the same, however, the RA-00AB model was softer than the RA-05AB model.

Table 4.1. The point dose at 0.5, 1.0 and 1.5 cm depth between commercial and in-house boluses.

Depth (cm)	Commercial (cGy)	RA-05AB (cGy)	RA-00AB (cGy)
0.5	209.3	209.8	209.8
1.0	206.7	206.5	206.1
1.5	202.3	201.9	201.6

Moreover, the planar dose differences were also evaluated at 1.5 cm depth using gamma index from SNC-patient software, as shown in figure 4.1.
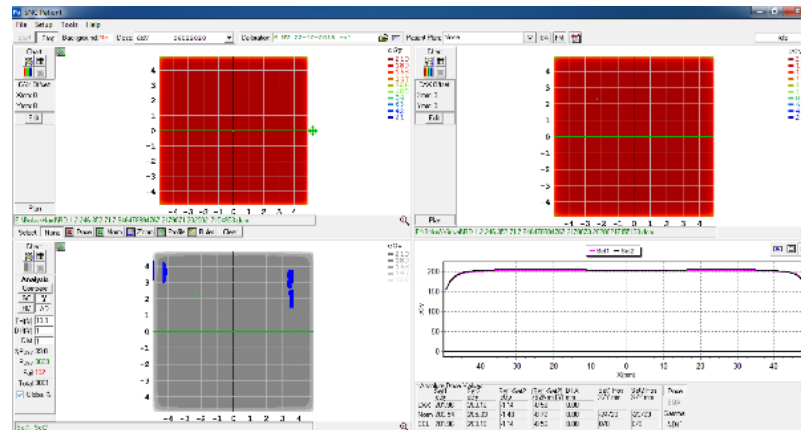
Figure 4.1: The planar dose differences at 1.5 cm depth using gamma index from SNC-patient software.

The planar dose differences were also presented the excellent agreement with 100% pass rate at 3%/2 mm gamma criteria in both types of the bolus. However, two types of silicone rubber bolus were also presented good dosimetric properties. For the physical property, the hardness of the RA-00AB model and the RA-05AB model were 1.5 and 5 HA, respectively. So, the RA-00AB model bolus was selected for the next step due to that was softer than the RA-05AB model.

4.1.1 Flat customized bolus fabrication

The flat customized bolus of RA-00AB model was fabricated by using the flat container with size of 30x30x1 cm^3 as shown in figure 4.2.
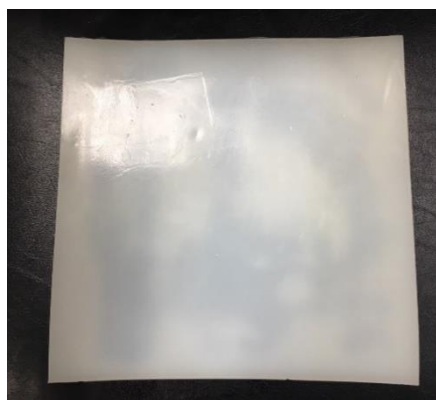

Figure 4.2: Flat customized bolus with size of 30x30x1 cm^3

4.1.2 3D customized bolus fabrication

The 3D customized bolus from RA-00AB model was fabricated in 3 pieces from 3 regions: nose, cheek, and neck. For the nose region bolus has a variation of thickness, especially in nose bridge region. However, the cheek and neck regions have relatively consistent of the thickness. The three pieces of 3D customized bolus are presented in figure 4.3.
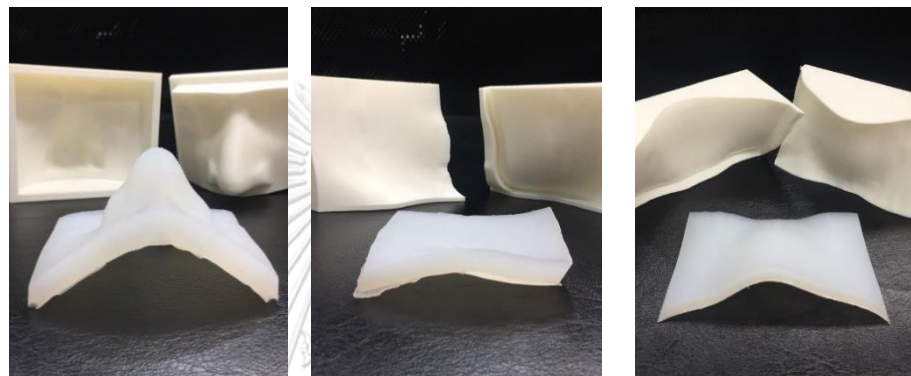

Figure 4.3: 3D customized bolus for difference regions
(a) nose region, (b) cheek region and (c) neck region

4.2 Bolus characteristics

The bolus characteristics of flat customized bolus from RA-00AB silicone rubber model with the size of 30x30x1 cm^3, such as thickness, density, Hounsfield unit (HU), and dose attenuation, were also confirmed and compared to commercial flat bolus. The physical properties of two types of boluses, commercial bolus and customized bolus, were compared. The average thickness of commercial bolus was 1.05±0.00 cm, while customized bolus was 1.07±0.01 cm. The density of commercial bolus and customized bolus were 1.03 and 0.99 g/cm^3, respectively. The HU of commercial bolus and customized bolus were -124.00±63.33 and -73.00±42.57, respectively. There were good agreements between the dose attenuation at 5 cm depth within solid water phantom that commercial bolus and customized bolus were 167.2 and 167.6, respectively. The point dose differences were only 0.2%.

The ATR-FTIR Test was used to compare the chemical compositions between irradiation bolus and non-irradiation bolus. The ATR-FTIR spectra were presented in the functional group of the bolus by evaluating percent transmittance in the range of middle infrared wavenumber. Figure 4.4 shows the overlapped spectra between irradiation bolus and non-irradiation bolus, indicating that the bolus compositions have not significantly changed when the bolus was irradiated with radiation. The curves show in superimposed; the curve of irradiation is shifted down to illustrate the same pattern of both spectrums.
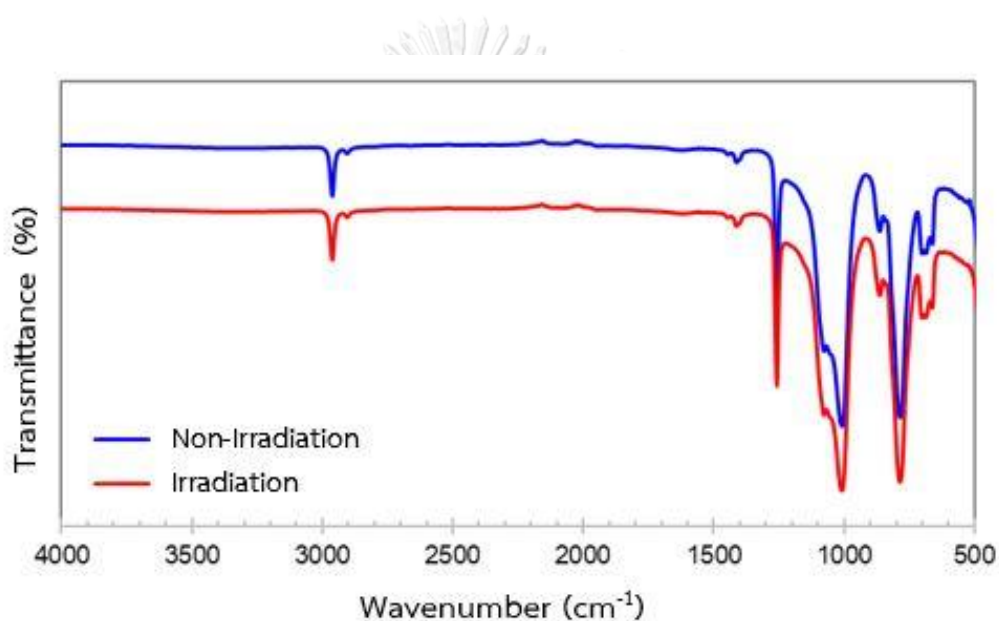

Figure 4.4: ATR-FTIR spectra of non-irradiation bolus and irradiation bolus.

The thermogravimetric analysis test was performed to evaluate the stability of the bolus after irradiation. There are two graphs; the first graph was the TGA graph that represented the mass loss as a function of temperature. Figure 4.5 shows that at around 450°C, the non-irradiation bolus showed a stepwise decrease in mass while the irradiation bolus showed a slight decrease. This may be due to the stronger chemical bond of bolus after irradiation, which led to more stability at that temperature.
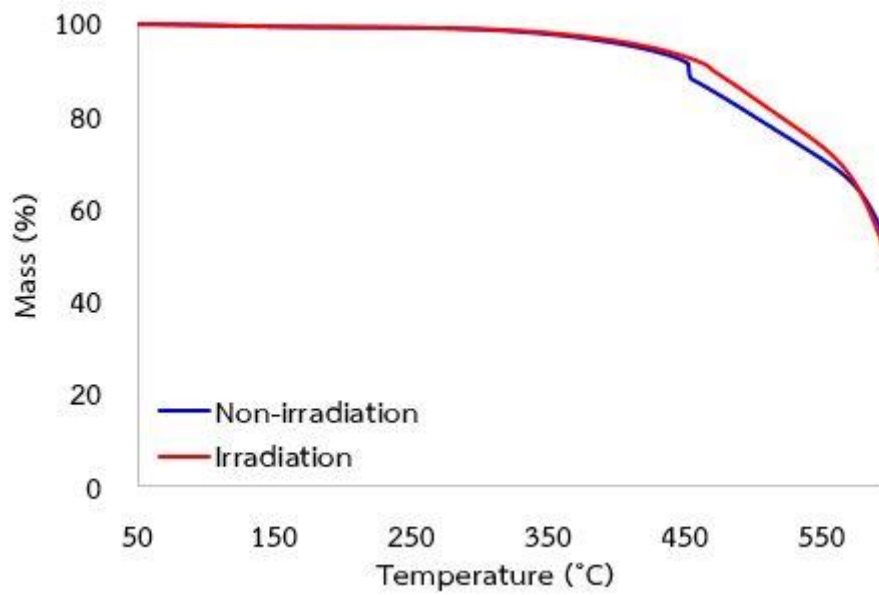
Figure 4.5: Thermogravimetric curves of non-irradiation and irradiation bolus.

The second graph was Derivative Thermogravimetry, or DTG graph. The graph was plotted between the rates of mass change and temperature. There was no change in mass during the analyzed period giving dm/dt to zero, and a peak of the DTG curve would occur when the mass change rate is the highest. The non-irradiation bolus showed a higher mass change rate than that of the irradiation bolus, as shown in figure 4.6. This is corresponding to the mass loss data; after irradiation, the bolus showed a slowly mass change rate compared to the non-irradiation bolus.
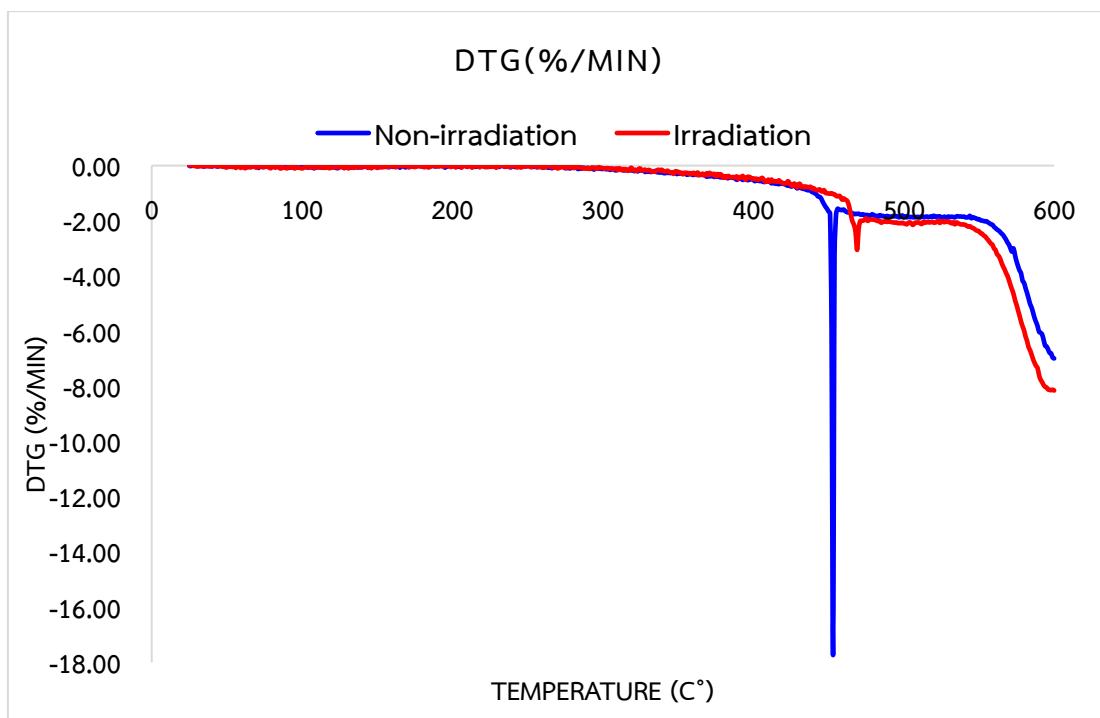
Figure 4.6: Derivative Thermo gravimetry test

However, the TGA and DTG curves were showed that a temperature that affects to change of mass in a range of 400-500 °C. So, boluses were not affected by room temperature in clinical use.

4.3 Clinical application

The clinical application consists into two parts, point dose difference and planar dose difference.

4.3.1 Point dose difference

The percentage dose differences between EBT3 film measurement along the central axis (3D customized bolus and commercial bolus) and virtual bolus calculation were calculated in 3 regions: nose, cheek, and neck by using virtual bolus created in TPS as a reference.

Figure 4.7 shows the percentage dose differences of 3D customized bolus and commercial bolus of nose region compared with virtual bolus data and the data presented the average dose differences of -0.19±2.77% and -0.24±2.76%, respectively. The differences were in line with the acceptability criteria of external dose calculations from IAEA TRS 430.
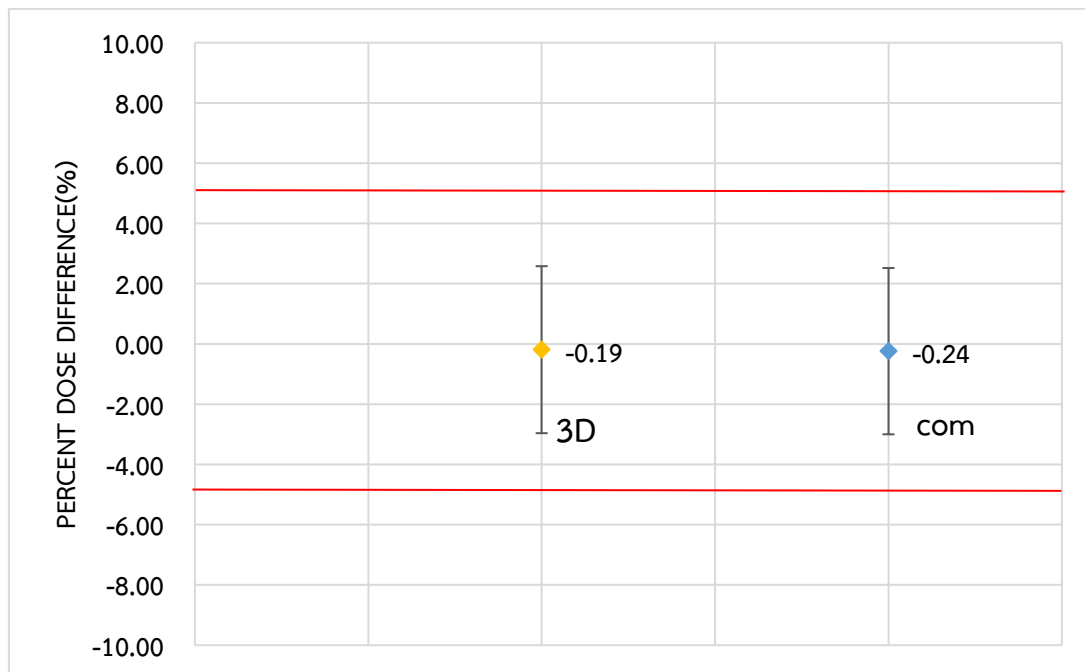

Figure 4.7: The percentage dose difference of nose region

The paired t-test was selected to compare the percentage dose differences between 3D customized bolus and commercial bolus, which p-valued = 0.783 signify that 3D customized bolus was not different from commercial bolus.

Figure 4.8 presents the percentage dose differences of 3D customized bolus and commercial bolus compared with virtual bolus in the cheek region that showed the average dose differences of -3.48±4.21% and -4.65±4.16%, respectively. Even though the differences rather differ from virtual bolus but it was still in the acceptability criteria of external dose calculations from TRS 430.
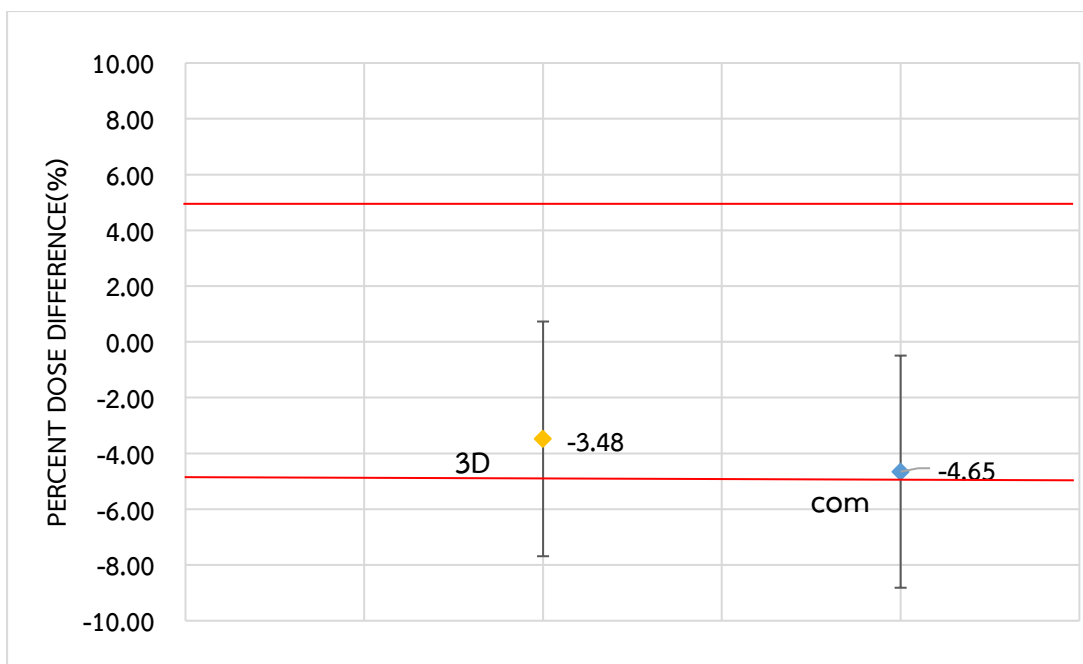
Figure 4.8: The percentage dose difference of cheek region

The paired t-test was used to compare the percentage dose differences between 3D customized bolus and commercial bolus, which p-valued = 0.001 signify that 3D customized bolus differs from commercial bolus due to placed position and the direction of the beam according to inhomogeneity region.

Finally, figure 4.9 shows the percentage dose differences of 3D customized bolus and commercial bolus compared with virtual bolus in the neck region. The average dose differences of 3D customized bolus and commercial bolus compared with virtual bolus were 0.28±1.80% and -0.09±2.18%, respectively. These small differences were within the acceptability criteria of external dose calculations from TRS 430.
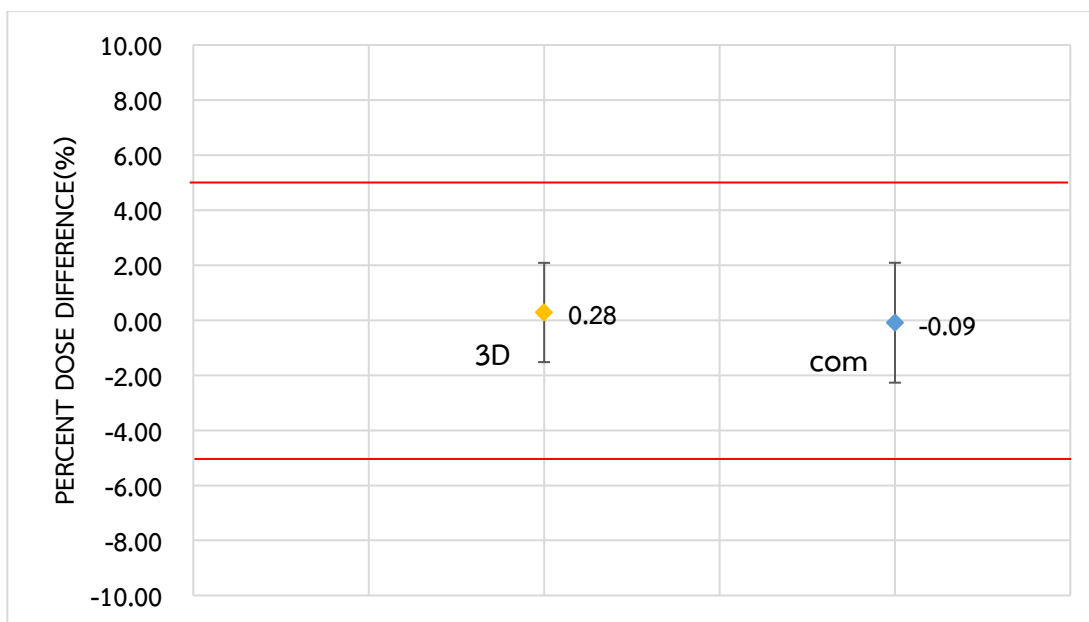
Figure 4.9: The percentage dose difference of neck region

The paired t-test was used to compare the percentage dose differences between 3D customized bolus and commercial bolus, which p-valued = 0.016 signify that 3D customized bolus differs from commercial bolus.

4.3.2 Planar dose difference

The SNC patient software program was used to compare planar dose differences by evaluating the percent gamma passing rate at 3%/2 mm and 10% threshold, which the virtual bolus plan referred to.

For the nose region, the average planar dose difference of commercials bolus and 3D customized were 88.15% and 90% gamma passing rate, respectively. The dose differences of commercial bolus are shown in figure 4.10, which clearly indicate the large air gaps compared to virtual bolus.
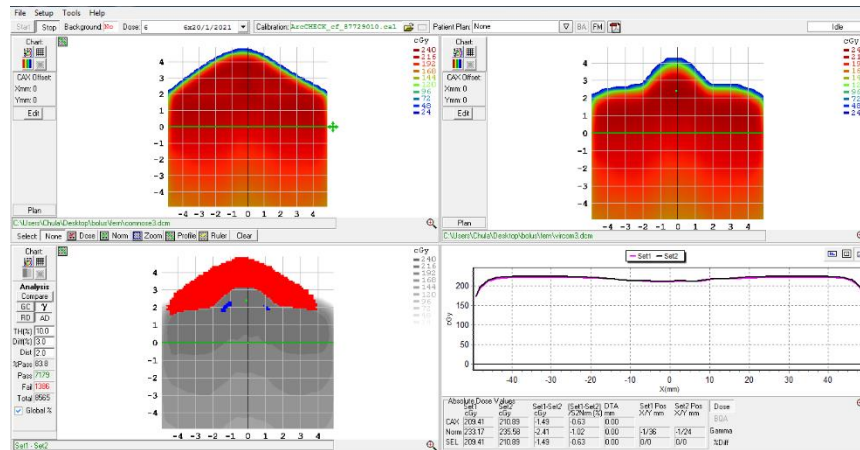
Figure 4.10: The planar dose difference of nose region with commercial bolus

Figure 4.11 shows the planar dose differences between 3D customized bolus and virtual bolus. The large air gaps were reduced by using a 3D customized bolus in addition to has a similar shape as the virtual bolus.
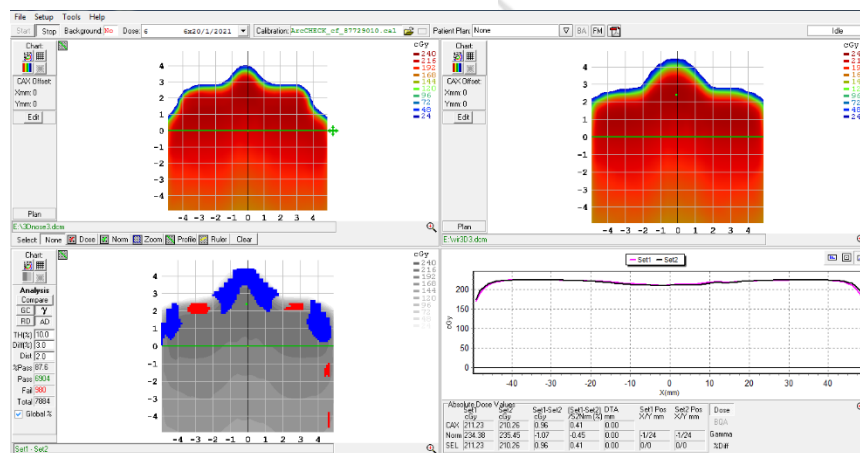

Figure 4.11: The planar dose difference of nose region with 3D customized bolus

However, the difference was presented in region of the bolus, which is the buildup region because of the variation of shape and thickness of 3D customized bolus.

The average planar dose difference of commercials bolus and 3D customized in the cheek region was 91.7% and 92.4% gamma passing rate, respectively. The dose differences of commercial bolus are shown in figure 4.12, which clearly indicated the significant air gaps compared to virtual bolus.
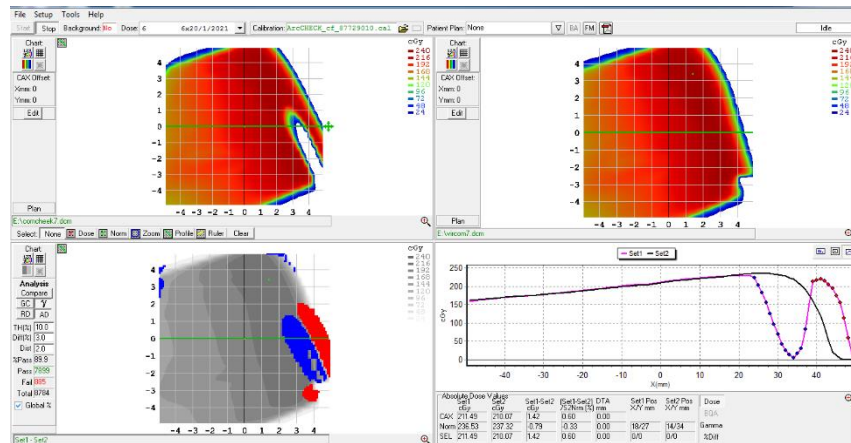
Figure 4.12: The planar dose difference of cheek region with commercial bolus

Figure 4.13 shows the planar dose differences between 3D customized bolus and virtual bolus. The large air gaps were reduced by using a 3D customized bolus in addition to has the similar shape as the virtual bolus.

Figure 4.13: The planar dose difference of cheek region with 3D customized bolus

However, the dose difference was shown in the region of the bolus, which buildup region because of the variation of shape, thickness including the size of a 3D customized bolus.

For the neck region, the average planar dose difference of commercials bolus and 3D customized were 95.8% and 99.45% gamma passing rate, respectively. The

dose differences of commercial bolus are shown in figure 4.14, which clearly indicate the large air gaps compared to virtual bolus.
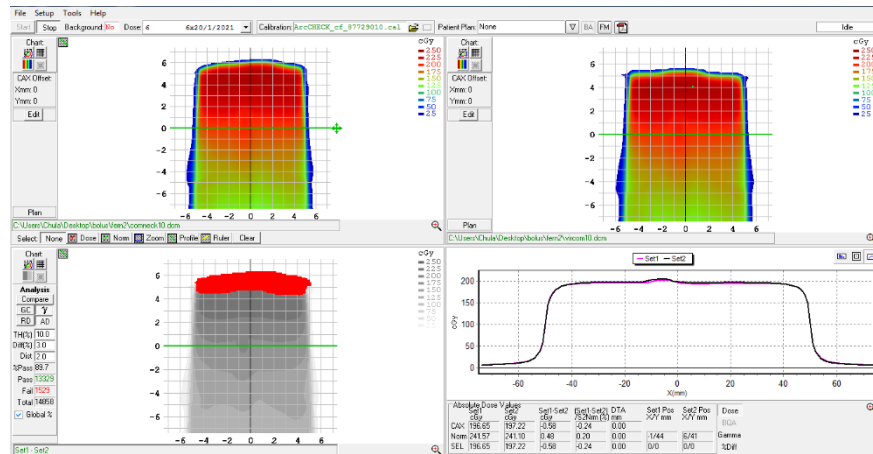
Figure 4.14: The planar dose difference of neck region with commercial bolus

Figure 4.15 shows the planar dose differences between 3D customized bolus and virtual bolus. The large air gaps were reduced by using a 3D customized bolus in addition to has the similar shape as the virtual bolus.
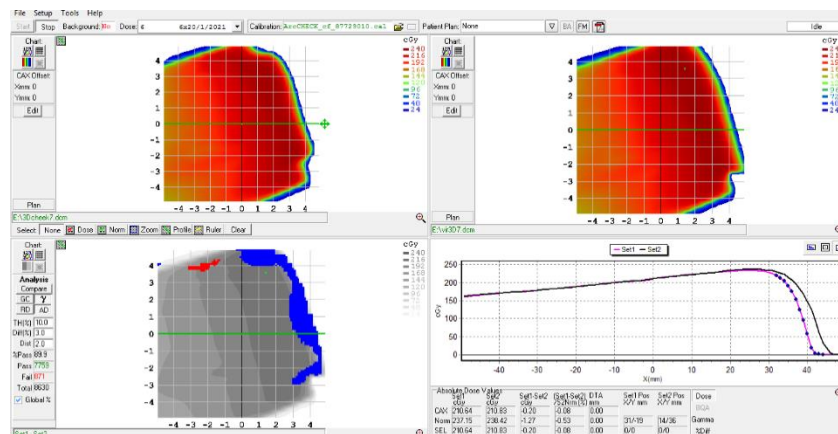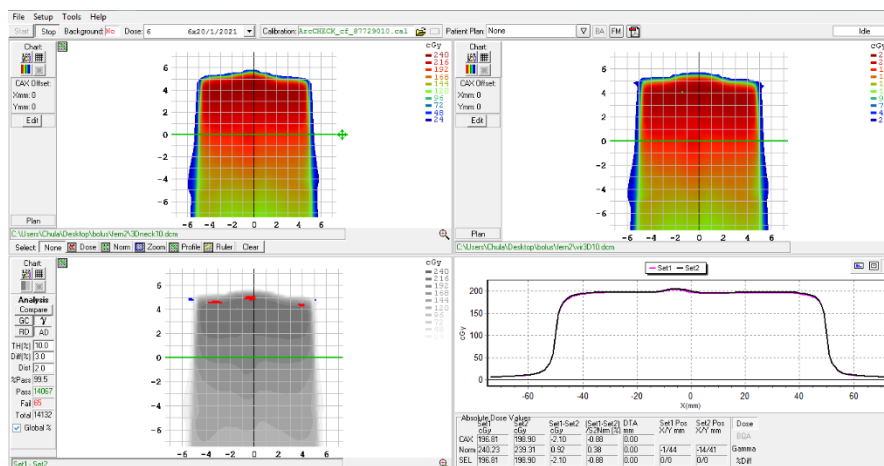

Figure 4.15: The planar dose difference of neck region with 3D customized bolus

However, the small air gap presented in the region between the 3D customized bolus and phantom because of the variation of shape and placed position of the 3D customized bolus.

CHAPTER V

DISCUSSION AND CONCLUSION

5.1 Discussion

5.1.1 Bolus fabrication

The two models of silicone rubber, the RA-00AB model and RA-05AB model were presented in good agreement with point dose differences; both types of bolus showed less than 0.4% deviation from the commercial for all depths. At the same time, the gamma passing rate at 3%/2mm gamma criteria was also presented the excellent agreement with 100% pass rate in both types of the bolus, however, the hardness which a part of the physical property of boluses was evaluated by shore A. The hardness of the RA-00AB model was 1.5 HA imply that the RA-00AB model softer than RA-05AB which 5 HA. So that, RA-00AB silicone rubber bolus represented to contact to the surface than another model.

5.1.2 Bolus characteristics

When the size of 30×30×1 cm^3 of RA-00AB bolus was fabricated, the physical characteristics were quite the same as a commercial bolus for all properties of thickness, density, Hounsfield unit (HU), and dose attenuation that means the RA-00AB silicone rubber can be replaced the commercial super flab bolus. However, commercial super flab bolus has limitations in case of irregular shape surface.

The 3D printing technology has been applied to create individually customized bolus designed to compensate for the irregular surface of patient in radiotherapy. In general, two ways have been reported of making a bolus in past studies. One method was to directly print a bolus with 3D printing materials after the design stage. Polylactic acid (PLA) was a commonly used printing material, which had been demonstrated to be a bolus material in a previous study[11]. Studies reported that the doses of 3D printed PLA bolus in phantom simulating radiotherapy of breast

cancer after radical resection were more uniform than with the commercial bolus[12, 13]. Acrylonitrile butadiene styrene (ABS) copolymer is another printing material commonly used except PLA, but both materials are too hard and have poor comfort. Another method is to print the shell of the bolus and then fill it with other soft materials that our study uses this method. Richard R et.al.[14] printed the shell in PLA using the 3D printer and filled it with silicone rubber for non‑melanoma skin cancer electron beam radiotherapy. Silicone rubber has the advantage when making a bolus due to its excellent biocompatibility, chemical stability, and good mechanical properties, but its density is $1.1–1.2$ g/cm^3 which differs from that of human tissue. In this study, our silicone rubber as filling materials was better than their studied with of the 0.99 g/cm^3.

5.1.3 Clinical application

Although the 3D customized bolus has a variation of shape and thickness, the 3D printed bolus was a very good fit against the irregular surface of the RANDO phantom that can significantly reduce the air gap between bolus and phantom compared with commercial bolus. With the bolus, the skin dose was increased that showed the same result as Shin WK et al. [19], who fabricated a customized 3D bolus using a 3D printer and evaluated its feasibility in clinical practice by comparing its performance without a bolus in the treatment planning system and also the same result of Jae WP et al., [29] who fabricated a customized 3D bolus using a 3D printer and compared feasibility in clinical practice by comparing its performance without a bolus and with that of a commercial flat bolus. It means that the 3D printed customized bolus is a good buildup material. Furthermore, the treatment plan with the 3D printed customized bolus could be clinically effective, help to overcome the problem of variable air gaps, and improve the reproducibility of daily setup conditions on irregular surfaces compared to commercial flat boluses.

5.2 Conclusion

In radiotherapy, the commercial boluses have different degrees of gaps because of their poor shape on the irregular surface. The effect of the air gap on surface dose reduction is related to factors. In practice for some cases, the small pieces of commercial bolus were cut to use with some regions of the patient, which is not economical. So, the use of three-dimensional (3D) printing technology could help to create a patient specific bolus. There are several materials to fabricate 3D customized bolus, but material is too hard and with poor comfort. Then the silicone rubber RA-00AB model was used to fabricate as a 3D customized bolus. A silicone rubber bolus produced a commercial bolus's feasible physical and dosimetric properties and could save cost compared to a commercial bolus. The 3D printed customized bolus is a good buildup material and could potentially replace and improve commercially flat bolus and increase the radiotherapy's efficacy.

จุฬาลงกรณ์มหาวิทยาลัย
CHULALONGKORN UNIVERSITY

REFERENCES

1. Vyas, V., et al., *On bolus for megavoltage photon and electron radiation therapy.* 2013. **38**(3): p. 268-273.

2. Khan, F.M. and J.P. Gibbons, *Khan's the physics of radiation therapy.* 2014: Lippincott Williams & Wilkins.

3. Benoit, J., et al., *Effect of wetness level on the suitability of wet gauze as a substitute for superflab® as a bolus material for use with 6 MV photons.* 2009. **50**(5): p. 555-559.

4. Butson, M.J., et al., *Effects on skin dose from unwanted air gaps under bolus in photon beam radiotherapy.* 2000. **32**(3): p. 201-204.

5. Khan, Y., et al., *Clinical and dosimetric implications of air gaps between bolus and skin surface during radiation therapy.* 2013. **4**(7): p. 1251.

6. Kong, M., L.J.A.P. Holloway, and E.S.i. Medicine, *An investigation of central axis depth dose distribution perturbation due to an air gap between patient and bolus for electron beams.* 2007. **30**(2): p. 111-119.

7. Sharma, S. and M.J.M.p. Johnson, *Surface dose perturbation due to air gap between patient and bolus for electron beams.* 1993. **20**(2): p. 377-378.

8. Ju, S.G., et al., *New technique for developing a proton range compensator with use of a 3-dimensional printer.* 2014. **88**(2): p. 453-458.

9. Schubert, C., M.C. Van Langeveld, and L.A.J.B.J.o.O. Donoso, *Innovations in 3D printing: a 3D overview from optics to organs.* 2014. **98**(2): p. 159-161.

10. Ziegler, E.a., *Superflap Bolus [Internet].* **[cited 2020 Nov 26]. Availiable from:https://www.bebig.com/home/products/radiotherapy_accessories/superflab/**.

11. Burleson, S., et al., *Use of 3D printers to create a patient-specific 3D bolus for external beam therapy.* 2015. **16**(3): p. 166-178.

12. Ha, J.-S., et al., *Customized 3D printed bolus for breast reconstruction for modified radical mastectomy (MRM).* 2016. **27**(4): p. 196-202.

13. Park, S.-Y., et al., *A patient-specific polylactic acid bolus made by a 3D printer for breast cancer radiation therapy.* 2016. **11**(12): p. e0168063.

14. Ricotti, R., et al., *Dosimetric characterization of 3D printed bolus at different infill percentage for external photon beam radiotherapy.* 2017. **39**: p. 25-32.

15. Digitaltrends, *Three dimentional printing thehnological [Internet].* **[cited 2020 Nov 27]. Available from:https://www.digitaltrends.com/computing/what-is-3d-printing/**.

16. Depuydt, T., et al., *A quantitative evaluation of IMRT dose distributions: refinement and clinical assessment of the gamma evaluation.* 2002. **62**(3): p. 309-319.

17. Varatharaj, C., et al., *Dosimetric verification of brain and head and neck intensity-modulated radiation therapy treatment using EDR2 films and 2D ion chamber array matrix.* 2010. **6**(2): p. 179.

18. Low, D.A. and J.F.J.M.p. Dempsey, *Evaluation of the gamma dose distribution comparison method.* 2003. **30**(9): p. 2455-2464.

19. Kim, S.-W., et al., *A customized bolus produced using a 3-dimensional printer for radiotherapy.* 2014. **9**(10): p. e110746.

20. Kong, Y., et al., *A dosimetric study on the use of 3D-printed customized boluses in photon therapy: A hydrogel and silica gel study.* 2019. **20**(1): p. 348-355.

21. Okay, O. and W.J.M. Oppermann, *Polyacrylamide– clay nanocomposite hydrogels: rheological and light scattering characterization.* 2007. **40**(9): p. 3378-3387.

22. Shibayama, M., et al., *Small-angle neutron scattering study on uniaxially stretched poly (N-isopropylacrylamide)– clay nanocomposite gels.* 2005. **38**(26): p. 10772-10781.

23. Yang, J., et al., *Synthesis and characterization of mechanically flexible and tough cellulose nanocrystals–polyacrylamide nanocomposite hydrogels.* 2013. **20**(1): p. 227-237.

24. Yang, J., et al., *Simple approach to reinforce hydrogels with cellulose nanocrystals.* 2014. **6**(11): p. 5934-5943.

25. Du, G., et al., *Tough and fatigue resistant biomimetic hydrogels of interlaced self-assembled conjugated polymer belts with a polyelectrolyte network.* 2014. **26**(11): p. 3522-3529.

26. Gao, G., et al., *Tough nanocomposite double network hydrogels reinforced with clay nanorods through covalent bonding and reversible chain adsorption.* 2014. **2**(11): p. 1539-1548.

27. Hu, Z. and G.J.A.m. Chen, *Novel nanocomposite hydrogels consisting of layered double hydroxide with ultrahigh tensibility and hierarchical porous structure at low inorganic content.* 2014. **26**(34): p. 5950-5956.

28. Adamson, J.D., et al., *Characterization of water-clear polymeric gels for use as radiotherapy bolus.* 2017. **16**(6): p. 923-929.

29. Park, J.W., et al., *Fabrication of malleable three-dimensional-printed customized bolus using three-dimensional scanner.* 2017. **12**(5): p. e0177562.

30. Varian, *EclipseTM Treatment Planning System [Internet].* **[cited 2020 Dec 04]. Available from:https://www.varian.com/products/radiotherapy/treatment-planning/eclipse**.

31. Stasi, M., et al., *Pretreatment patient-specific IMRT quality assurance: a correlation study between gamma index and patient clinical dose volume histogram.* 2012. **39**(12): p. 7626-7634.

32. LABORATORIES, R., *Fourier Transform Infrared Spectroscopy [Internet].* **[cited 2020 Nov 14]. Available from:https://rtilab.com/techniques/ftir-analysis/**.

33. Wikipedia, *Thermogravimetric analysis or thermal gravimetric analysis [Internet].* **[cited 2020 Nov 14]. Available from: https://en.wikipedia.org/wiki/Thermogravimetric_analysis**.

APPENDIX

The approval of institutional review board

Certificate approval from institutional review board (IRB) of Faculty of Medicine, Chulalongkorn University, Bangkok, Thailand.

Figure A: The approval of institutional review board

VITA

NAME   Nichakan Chatchumnan

DATE OF BIRTH   6 April 1997

PLACE OF BIRTH   Bangkok, Thailand

INSTITUTIONS ATTENDED   Bachelor of Science, Department of Physics, Faculty of
                        Science, Chulalongkorn University, Bangkok, Thailand

PUBLICATION   Chatchumnan N, Kingkeaw S, Aumnate C, and
                        Sanghangthum T. Development and dosimetric verification
                        of 3D customized bolus in radiotherapy. In Proceedings of
                        20th Asia-Oceania Congress on Medical Physics (AOCMP) -
                        18th South-East Asia Congress of Medical Physics
                        (SEACOMP) - 12th Annual Meeting of Thai Medical
                        Physicist Society (TMPS), Phuket, Thailand, 2020